JPRS L/8936

21 February 1980

USSR Report

PHYSICS AND MATHEMATICS

(FOUO 2/80)

FBIS FOREIGN BROADCAST INFORMATION SERVICE

APPROVED FOR RELEASE: 2007/02/08: CIA-RDP82-00850R000200050038-3

NOTE

JPRS publications contain information primarily from foreign newspapers, periodicals and books, but also from news agency transmissions and broadcasts. Materials from foreign-language sources are translated; those from English-language sources are transcribed or reprinted, with the original phrasing and other characteristics retained.

Headlines, editorial reports, and material enclosed in brackets [] are supplied by JPRS. Processing indicators such as [Text] or [Excerpt] in the first line of each item, or following the last line of a brief, indicate how the original information was processed. Where no processing indicator is given, the information was summarized or extracted.

Unfamiliar names rendered phonetically or transliterated are enclosed in parentheses. Words or names preceded by a question mark and enclosed in parentheses were not clear in the original but have been supplied as appropriate in context. Other unattributed parenthetical notes within the body of an item originate with the source. Times within items are as given by source.

The contents of this publication in no way represent the policies, views or attitudes of the U.S. Government.

For further information on report content call (703) 351-2938 (economic); 3468 (political, sociological, military); 2726 (life sciences); 2725 (physical sciences).

APPROVED FOR RELEASE: 2007/02/08: CIA-RDP82-00850R000200050038-3

JPRS L/8936

21 February 1980

USSR REPORT

PHYSICS AND MATHEMATICS

(FOUO 2/80)

This serial publication contains articles, abstracts of articles and news items from USSR scientific and technical journals on the specific subjects reflected in the table of contents.

Photoreproductions of foreign-language sources may be obtained from the Photoduplication Service, Library of Congress, Washington, D.C. 20540. Requests should provide adequate identification both as to the source and the individual article(s) desired.

CONTENTS PAGE

CONTENTS (Continued) Page

PHYSICS

LASERS AND MASERS

UDC 621.375.826+533.6.011

THE GAIN AT THE 00°1-10°0 TRANSITION OF CO_2 IN A REACTING FLOW OF A GAS MIXTURE CONTAINING CO AND N_2O

Moscow KVANTOVAYA ELEKTRONIKA in Russian Vol 6 No 11, 1979 manuscript received 18 Mar 78 pp 2439-2441

[Article by A.I. Didyukov, A.S. D'yakov, N.N. Ostroukhov, B.K. Tkachenko and Ye.M. Cherkasov, Moscow Physics and Engineering Institute]

[Text] A scheme for supersonic and subsonic blasts of cold N_2O into a heated mixture of gases containing CO is studied. This scheme permits a steady-state exothermic reaction with the formation of CO_2 molecules. It is found that the greatest gain (≈ 1%/cm) is realized when blowing N_2O into the subsonic portion of a flow of N_2-CO-He. Replacing the He with hydrogen or water vapors reduces the gain. Analysis indicates the possible contribution to the gain of vibrationally excited CO_2 molecules, formed as a result of the reaction.

The possibility of using nonequilibrium chemical reactions to produce the active medium of a CO_2-N_2 laser was indicated in paper [1]. The results of [2, 3] which were subsequently achieved can be explained by the presence of supplemental chemical pumping of the upper CO_2 lasing level as the result of an exothermal oxidation reaction of CO in the critical cross-section region of the nozzle.

We studied the reaction of carbon monoxide with nitrous oxide, which is realized when cold N_2O (T_0 = 300° K) is blown into a heated mixture of gases containing CO. This scheme makes it possible in principle, to realize a steady-state flow mode with nonequilibrium exothermal reactions to form the active lasing medium.

We studied two blow-in variants: in the supersonic and the subsonic channels of the nozzle. An advantage of the first is the better conditions for freezing the vibrational energy, however, the initiation and course of the chemical reactions in this case is made difficult of the low density and onset temperature, which significantly increase the

reaction delay time. In the case of blow-in into the subsonic portion of the flow, the conditions for mixing and the course of the reactions are improved. Condsidering the fact that at the same density, the relaxation and reaction rates are basically determined by the onset and vibrational temperatures respectively, and by a careful selection of the blow-in point, one can assure the conditions for the nonequilibrium exothermal reaction and assure effective freezing of the energy liberated in the expanding flow.

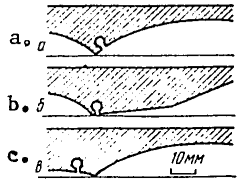

Figure 1. The configurations of the nozzles used: a. Nozzle 1 with injection into the superconic section, $h^* = 0.35$ mm, the injection coordinate $X_{in} = 2.2$ mm, the probe coordinate $X_p = 25$ mm; b. Nozzle II with injection into the supersonic section, $h^* = 0.5$ mm, the aperture half-angle is $\Theta = 5°$, $X_{in} = 0.5$ mm, $X_p = 70$ mm; c. Nozzle III with injection in the subsonic section, $h^* = 0.35$ mm, $X_{in} = -13$ mm, $X_p = 3-$ mm.

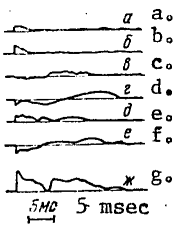

Figure 2. Oscilloscope traces of the intensity, registered in the region $\lambda = 10.6$ micrometers.

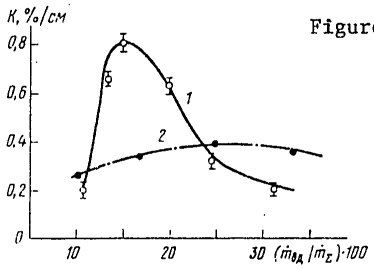

Figure 3. The gain as a function of the ratio of the rates of flow $\dot{m}_{in}$ of the N_2O (1) and CO_2 (2) being blown in to the overall flow rates $\dot{m}_\Sigma$ for the case of injection into the helium containing mixture (nozzle 3).

The experiments were performed on the set-up described in paper [4]. The profiles of the nozzles used are depicted in Figure 1. The N_2O was blown in through holes in the nozzle wall. In variants a and b, holes with

a diameter of 1 mm were spaced at intervals of 10 mm, in which case, the series of holes in one half of the nozzle were shifted by 5 mm with respect to the series of the other half. In variant c, the diameter of the holes was 0.3 mm and the spacing between them was 5 mm; the gas was blown in from one half of the nozzle. The ratio of the flow rates of the gas being blown in and the main flow varied from 0.1 to 1.

The experiments were carried out with mixtures of 40% CO + 40% N_2 + 15% H_2 + + 5% H_2O and 40% CO + 20% N_2 + 40% He. For them, the radiation intensity of the gas flow in the region λ = 10.6 mm was evaluated (in a band singled out by a dispersion filter). In experiments without the blowing-in, the oscilloscope traces of the radiation intensity of the flow, together with the intensity of the probe laser and without it, are in agreement (Figure 2a). The oscilloscope trace of the flow intensity with the N_2O blown-in (Figure 2b) is similar to the first, however the maximum level of the signal is higher in this case.

Thus, signal amplification of the probe laser, recorded when the N_2O is blown-in, can be entirely explained by the formation of CO_2 in the chemical reactions.

We shall move on to a description of the results obtained with the blowing-in of N_2O in the case of the nozzle configurations which we selected. In experiments with nozzle I (see Figure 1a), no amplification was recorded over the entire length of the nozzle when working with both mixtures. This negative result, apparently, is explained by the fact that the chemical reaction delay time is greater than the flow time of the gaseous mixture from the blow-in point to the mozzle edge.

Nozzle II (see Figure 1b) permited a reduction in the difference between these times because of decrease in the flow rate and an increase in the density and temperature. An oscilloscope trace of the trial when N_2O was blown into a mixture containing H_2 and H_2O is shown in Figure 2c. A gain of about 0.4%/cm was registered. For comparison, experiments were conducted with CO_2 blown-in, other conditions being the same (Figure 2d). The maximum gain likewise reached about 0.4%/cm, however, the time curve was different. The gain when N_2O is blown-in begins sharply somewhat earlier and sharply terminates. when CO_2 is blown-in, absorption is initially observed, which then smoothly goes over to amplification. The maximum in the gain is achieved at that point in time when the gain for the case of N_2O being blown-in terminates. Even considering the fact that in the oxidation reaction of CO, the N_2O is completely expended and the partial quantities of CO_2 in the former (see Figure 2c) and in the latter (see Figure 2d) cases are identical, a conclusion can be drawn concerning the chemical pumping of the upper lasing level. However, for a complete and precise assessment of the influence of the chemical reactions, it is necessary to monitor the concentration of CO_2, which is formed as a result of the chemical reactions of CO with N_2O. This monitoring was not done in this work. In the experiments with the second mixture, no gain was registered. We believe that

this is related to a lower reaction rate in the absence of H_2 and water vapor in the mixture, something which was indicated in [5].

In experiments where nitrous oxide was blown-in ahead of the critical cross-section of the nozzle (the profile of Figure 1c), a gain was registered for both mixtures. For a hydrogen containing mixture, the gain reached approximately 0.3%/cm (Figure 2e). This result is comparable to that obtained when CO_2 is blown-in (Figure 2f). A significant increase in the gain was observed when N_2O was blown into a mixture in which the hydrogen was replaced by helium (Figure 2g). In these experiments, the maximum gain reached about 1%/cm. This is apparently due to the closer to optimal conditions for the course of the reaction and to the effective freezing of the liberated energy. It is necessary to note the difference in the nature of the oscilloscope traces obtained for injection in the supersonic and subsonic portions of the nozzle. In the oscilloscope traces of Figures 2e and g, there is a valley in the intensity of the registered radiation, which is due to the specific features of the injection process. The gas being blown in begins to get into the main flow when the pressure in the main injection line (20-30 atm) and the static pressure in the main flow are comparable. The pressure of the main flow in this case varies from 45 atm to 0.

A curve was obtained for the gain as a function of the amount of N_2O blown-in (Figure 3), which was limited by the conditions under which the experiment was conducted. Gain appeared at minimal injection, and with an increase in the injection, increases rapidly, reaching a maximum and then falling off sharply. This nature of the function, in our opinion is related to the critical conditions for the course of the nonequilibrium reactions.

Thus, the results obtained attest to the possibility of chemical pumping of the upper lasing level of the CO_2 molecule as a result of the occurrence of nonequilibrium exothermal reactions of CO with N_2O in a steady-state gas flow. The results of the studies allow for the hope that by a careful selection of the injection point, the structural design of the nozzle and the composition of the mixture, one can significantly increase the efficiency of the given scheme.

BIBLIOGRAPHY

1. I.S. Zaslonko, S.M. Kogarko, Yu.V. Chirikov, ZHURN. PRIKL. MEKH. I TEKHN. FIZ. [JOURNAL OF APPLIED MECHANICS AND ENGINEERING PHYSICS], No 2, p 48 (1973).

2. N.G. Basov, V.V. Gromov, Ye.P. Markin, A.N. Orayevskiy, A.K. Piskunov, D.S. Shapovalov, KVANTOVAYA ELEKTRONIKA, 3, 1154 (1976).

3. N.N. Kudryavtsev, S.S. Novikov, I.B. Svetlichnyy, DAN SSSR [REPORTS OF THE USSR ACADEMY OF SCIENCES], 231, 1113 (1976).

4. A.S. D'yakov, A.I. Didyukov, B.K. Tkachenko, Ye.M. Cherkasov, KVANTOVAYA ELEKTRONIKA, 5, 1166 (1978).

5. V.N. Kondrat'yev, Ye.Ye. Nikitin, "Kinetika i mekhanizm gazofaznykh reaktsiy" ["The Kinetics and Mechanism of Gas Phase Reactions"], Moscow, Nauka Publishers, 1974.

8225
CSO: 1862

LASERS AND MASERS

UDC 621.375.82

THE DEVASTATION OF THE LOWER LASING LEVEL OF CO_2 GAS DYNAMIC LASERS UNDER CONDITIONS OF A CHEMICALLY NONEQUILIBRIUM MEDIUM

Moscow KVANTOVAYA ELEKTRONIKA in Russian Vol 6 No 11, 1979 manuscript received 11 Jan 79 pp 2420-2421

[Article by N.Ya. Vasilik, A.D. Margolin and V.M. Shmelev, Institute of Chemical Physics of the USSR Academy of Sciences, Moscow]

[Text] It is experimentally demonstrated that in the working medium of CO_2 gas dynamic lasers, which operate on the combustion products of mixtures with an atomic composition of C, O, N, effective deactivation of the lower lasing level occurs with the collision of CO_2 molecules and NO molecules, which are formed in the decay of the original substances, while collisions with carbon monoxide molecules do not provide for effective deactivation of the lower lasing level.

In GDL's [gas dynamic lasers], operating on the combustion porducts of mixtures having an atomic composition of C, N, O, H, water vapors are used to devastate the lower lasing level. However, during collisions with water molecules, a considerable portion of the vibrational energy is lost. These losses are particularly pronounced when molecules of carbon monoxide are used as the vehicle for the vibrational energy [1].

The purpose of this work is to study the deactivation of the lower lasing level of CO_2 GDL's for the case of collisions of CO_2 molecules with CO and NO molecules. High values are given in the literature [2 - 5] for the probabilities of these processes.

The experiments were carried out with a setup consisting of a combustion chamber with a volume of 0.5 liters, a chamber ahead of the nozzle (0.4 liters) and a supersonic nozzle. The critical section dimensions were 0.3 x 300 mm. The expanding section of the nozzle was formed by the surface of a circular cylinder. The initial aperture half-angle of the nozzle was 30°. In the case of an expansion factor of 100 for the gas flow, the surface of the circular cylinder makes a tangential transition

to a plane, and in this way, the expanding section of the nozzle is coupled to a constant cross-section. The optical gain (or absorption) is determined by measuring the increase (or decrease) in the radiation of an electrical discharge laser in the constant cross-section channel at a distance of 90 mm from the critical section of the nozzle. The following mixtures were fed into the combustion chamber: $CO:O_2:N_2 = (3 + S):1.5:(7.5-X)$ and $CO:N_2O:N_2 = (3 \pm X):3:(6 \mp X)$, $0 \leq X \leq 1.5$. Commercial grade nitrogen and carbon monoxide, and medical grade oxygen and nitrous oxide were used in making the mxitures. The major equilibrium combustion products of these mixtures are CO_2 (25 - 30% of the volume), CO (up to 15%) and nitrogen.

The gas pressure in the constant cross-section supersonic channel and in the pre-nozzle chamber was measured by induction transducers. The maximum pressure values in the pre-nozzle chamber reached 40-50 atm, and in the constant cross-section channel, 8-10 mm Hg.

Experiments with the original $CO-O_2-N_2$ mixture showed that in the case of collisions of the CO_2 molecules with carbon monoxide molecules, effective relaxation of the lower lasing level does not occur, since the laser radiation is absorbed in the combustion products which contain up to 15% carbon monoxide (the white experimental circles in Figure 1), while the introduction of an insignificant amount of water vapor ($\approx$ 1%) into the composition of the working medium assures a positive gain (the black experimental point in Figure 1).

The optical gain α for the given mixture, obtained by numerical integration of the system of kinetics equations for the vibrational relaxation and gas dynamic equations, similar to the system in [10], where the presence of water vapors (curve 3 in Figure 1) is in quantitative agreement with experimental data. The values of α for water free mixtures consisting of CO_2, N_2 and CO were computed for two different functions of the temperature for the constant K(T) of the deactivation rate of the deformation type vibrations of the CO_2 molecules for the case of collisions with carbon monoxide molecules: curve 1 in Figure 1 corresponds to values of $K(T) = 10^4 - 10^5$ (mm Hg $\cdot$ sec)$^{-1}$ in a temperature range of 300-1,000° K [2 - 5], and curve 2 was obtained assuming the equality of the probabilities of the deactivation of the lower lasing level for the case of collisions with nitrogen and carbon monoxide molecules [6, 11].

A comparison of the results of experiments and calculations allows for the conclusion that the values of the deactivation constant K(T) in the literature [2 - 5] are substantially overstated.

Experimental values of the optical gain are given in Figure 2 for the combustion products of mixtures of $CO-N_2O-N_2$ (the small white circles), as well as in the combustion products of a control mixture of 2.9 CO + 0.1 C_2H_2 + 3.4N_2O + 5.6N_2 (the solid blacks circle). In this series of experiments, the combustion products of mixtures which do not contain water vapors amplified radiation with a wavelength of 10.6 micrometers.

Since the results of trials with $CO-O_2-N_2$ and $CO-N_2O-N_2$ mixtures, having the same atomic composition, and consequently, approximately the same equilibrium composition of the major combustion products, are different qualitatively, one can conclude that in the combustion products of hydrgen free mixtures of ($CO-N_2O-N_2$), deactivation of the lower lasing level occurs with collisions with chemically nonequilibrium products.

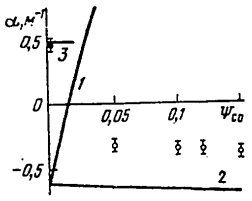

Figure 1. The optical gain as a function of the molar concentration of carbon monoxide in the combustion products.

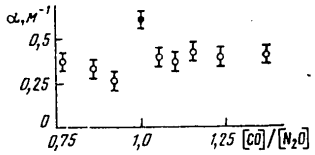

Figure 2. The optical gain as a function of the ratio of the molar concentrations of carbon monoxide and nitrous oxide in the original mixture.

The oxidation of carbon monoxide and the decay of nitrous oxide in the $CO + N_2O$ at temperatures of 1,500-2,000° K, runs according to the following scheme [7 - 9]:

$$N_2O+M\rightarrow N_2+O,$$
$$N_2O+O\rightarrow 2NO,$$
$$N_2O+O\rightarrow O_2+N_2,$$
$$N_2O+CO\rightarrow CO_2+N_2,$$
$$O+CO+M\rightarrow CO_2+M.$$

The yield of nitric oxide in the mixture of N_2O with CO at a temperature of 2,000° K amounts to about 30% of the N_2O [9].

At a temperature of 2,000° K and a pressure of 10 atm, the nitric oxide has a characteristic lifetime τ_1, which exceeds the time τ_2 of the presence of the reaction products in the combustion chamber of a GDL under the conditions of our experiments ($\tau_2 \approx 1$ msec). A high value of the probability P of the deactivation of the deformation vibrations of carbon dioxide gas molecules is given in the literature [4, 5] for the case of collisions with nitric oxide molecules ($P = 4 \cdot 10^{-3}$) at room temperature. On the basis of what has been presented here, it can be assumed that the devastation of the lower lasing level in experiments with N_2O was assured by the collisions of CO_2 molecules with NO, and

possibly, with other oxides of nitrogen. It is also possible that it is specifically the presence of NO in the gas discharge plasma which explains the errors in the measurement of K(T) in papers [2, 3].

It is shown in this paper that in the working medium of a carbon dioxid GDL's, which operate on the combustion products of mixtures with an atomic composition of C, O, N, effective reactivation of the lower lasing level occurs in the case of collisions of CO_2 molecules with NO molecules, and possibly, with other oxides of nitrogen, formed in the decay of the original substances, while collisions with carbon monoxide molecules do not assure effective deactivation of the lower lasing level.

BIBLIOGRAPHY

1. V.M. Shmelev, N.Ya. Vasilik, A.D. Margolin, KVANTOVAYA ELEKTRONIKA, 1, 1711 (1974).

2. P.K. Cheo, IEEE J. QE-4, 587 (1968).

3. M.C. Cower, A.I. Carswell, J. APPL. PHYS., 45, 3922 (1974).

4. I.M. Metter, PHYSIKALISCHE ZEITSCHRIFT SOWJETUNION [PHYSICS JOURNAL OF THE SOVIET UNION], 12, 233, (1937).

5. V.N. Kondrat'yev, "Kinetika khimicheskikh gazovykh reaktsiy" ["The Kinetics of Gas Chemical Reactions"], Moscow, Nauka Publishers, 1958.

6. I. Soto, S. Tsuchiya, J. PHYS. SOC. JAP., 33, 1120 (1972).

7. M.S. Lin, S.H. Bauer, J. CHEM. PHYS.,50, 3377 (1968).

8. D. Milks, R. Matula, "14th Symp. on Combustion", 1972,

9. I.S. Zaslonko, Ye.V. Mozzhukhin, Yu.K. Mukoseyev, V.N. Smirnov, FIZIKA GORENIYA I VZRYVA [COMBUSTION AND EXPLOSION PHYSICS], 14, 101 (1978).

10. A.S. Biryukov, TRUDY FIAN [PROCEEDINGS OF THE USSR ACADEMY OF SCIENCES INSTITUTE OF PHYSICS IMENI P.N. LEBEDEV], 83, 13 (1975).

11. M. Huetz-Aubert, G. Louis, J. Taine, PHYSICA, 93, No 2, 237, 1978.

8225
CSO: 1862

LASERS AND MASERS

UDC 621.378.33

ON THE OPTICAL EXCITATION OF A MOLECULAR LASER IN A PHOTODISSOCIATION WAVE PROPAGATING IN A DENSE GAS

Moscow KVANTOVAYA ELEKTRONIKA in Russian Vol 6 No 11, 1979 manuscript received 11 Feb 79 pp 2349-2360

[Article by I.A. Izmaylov and V.A. Kochelap, Institute of Semiconductors of the Ukrainian SSR Academy of Sciences, Kiev]

[Text] The photolysis of gaseous media which accompanies recombination reactions is studied. It is shown that with the action of high power radiation, such media are completely or partially bleached into nonsteady-state photochemical waves. Intense external radiation can produce large concentrations of atoms and radicals (10^{18} - 10^{19} cm^{-3}) and initiates strongly nonequilibrium reactions. The conditions for the formation of an inverse population of the electron states of the molecules - the recombination products - are studied for cases where the recombination reactions have a radition channel. Inversion can occur both with linear light absorption and in bleaching modes. The results are applied to a number of specific mixtures, for which the conditions for the occurrence of inversion and the light gains which occur are calculated.

Optical pumping [1] is widely used at the present time to excite electronic photo transition molecular lasers. This kind of pumping is quite universal, since it can be applied to various molecular systems, and is capable of initiating and sustaining processes which lead to an inverse population (direct population of the upper levels of the working photo transition, photodissociation with the formation of an excited molecule or atom, etc.). Of particular interest is the photolysis of a gas with subsequent chemical transformations which lead to excitation and an inverted population of the chemical reaction products. Thus, lasing was realized for the first time with the electron transition of a molecule excited during the course of an exchange chemical reaction [2, 3] (the $^1\Sigma_g^+ \rightarrow {}^3\Sigma_g^-$ in the S_2 molecule during the photolysis of COS).

An inverse population and light amplification can also arrive with the recombination of atoms and radicals: the products of photolysis. Such a possibility has been treated earlier in the literature [4, 5]. These and other studies have shown that when designing a recombination laser, it is necessary to take the following factors into account:

1. It is necessary to produce nonequilibrium concentrations of atoms and radicals of about 10^{18}--10^{19} cm^{-3}. This requires the application of high power light fluxes of the pumping light and the utilization of gases with high densities and absorption coefficients. Under these conditions, photolysis at a considerable depth is possible only in photochemical bleaching waves [6, 7].

2. Recombination reactions are one of the main chemical processes, which determine in many respects the nature of the photochemical waves which prove to be nonsteady-state and decaying.

3. With high concentrations of atoms and radicals, fast chemical reactions can also occur, which lead to the diminution of the active components, and which produce the molecules - the recombination products. These parasitic processes make it difficult, and in some cases, impossible, to produce an inverted population and achieve light gain.

4. In the case of absorption of the external light, considerable energy is liberated in the course of the subsequent chemical reactions, and the temperature increases and the inversion existence time falls off.

5. The high radiation powers which are delivered, are liberated in narrow spatial layers, lead to the appearance of large pressure gradients in the gas and cause the motion of the medium, something which complicates the photolysis picture and leads to optical inhomogeneity of the medium.

6. We took the factors cited above into account when constructing the theory of the optical excitation of an inverse population and light gain during the recombination reactions. The possibility of optical pumping of a recombination laser in a linear mode is treated (section 2), the nature of the bleaching waves in the recombining gas is studied (sections 3 and 4) and expressions are derived for the inverse population and light gain criteria. The results of the theory are applied to specific gas mixtures; the pressure and composition of the gas as well as the parameters of the light sources needed to excite lasers of the type considered here are computed (section 5).

1. The Initial Equations

The photolysis of a gas, which is accompanied by a bleaching wave and chemical transformation, is described by radiation transfer and chemical kinetics equations. These equations define the flux density of the photons of the actual frequencies J and the gas composition. The thermal

balance equation determines the gas temperature T. When the motion of the medium is taken into account, the gas density ρ and its velocity v are likewise to be determined. These cases will be specified separately.

We shall assume that all quantities depend on one spatial coordinate x, and the light propagates in a positive direction of x. Then the equation for J is written in the form

$$-\frac{1}{c}\frac{\partial J}{\partial t}+\frac{\partial J}{\partial x}=-W_J\equiv-\varkappa J, \qquad (1)$$

where κ is the light absorption coefficient, which depends on the composition and density of the gas. We shall assume that each act of light absorption leads to photodissociation. Equation (1) is applicable in two very interesting cases: for a monochromatic light source (laser pumping), where κ corresponds to the frequency of this light ω_L, and for radiation, the spectrum of which is considerably wider than the absorption spectrum which leads to the photolysis (pumping by a source with a brightness temperature of tens of thousands of degrees). In the second case, J is the flux of photons at frequencies which fall in the absorption band $\Delta\omega_L$; $\varkappa=\frac{1}{\Delta\omega_L}\int\limits_{\Delta\omega_L}d\omega\varkappa(\omega)$.

The kinetics equations can be written only for specific chemical processes. We shall consider two types of gaseous mixtures, which consist of donor molecules X and diluent molecules M of the atoms.

A. *The mixture of homonuclear X_2 and M molecules.* In this case, the photolysis

$$X_2+\hbar\omega_L\rightarrow 2X \qquad (2)$$

is accompanied by a single chemical process: the recombination reaction:

$$X+X+(M)=X_2+(M)+\begin{cases}\hbar\omega\\ Q_1,\end{cases} \qquad (I)$$

where Q_1 is the process heat for (I). In reaction (I), the presence of a radiation channel is assumed in addition to the thermal channel, where the radiation from the radiation channel can be used in lasers.

The concentrations [X] and $[X_2]$ are related by the relationship for the material balance: $[X_2] = (\rho/\rho_0)[X_2]_0 - 0.5[X]$, where the "0" subscript applies to the original gas, unperturbed by the light. The following equation is justified for [X]:

$$d[X]/dt=2W_J-(W_1-W_{1'}), \qquad (3)$$

where $W_J = \sigma[X_2]J$; W_1 and W_1' correspond to the direct and inverse processes of (1). Only those cases where the thermal dissociation processes can be neglected (the inverse process of (I)) will be treated below.

B. *The mixture of heteronuclear AX and M molecules.* In this case, besides the photolysis

$$AX+\hbar\omega_L \rightarrow A+X \tag{4}$$

recombination reactions (I) also occur as well as the following processes, initiated by the external radiation:

$$A+X+(M) \rightleftarrows AX+(M)+Q_2; \tag{II}$$

$$AX+X \rightleftarrows A+X_2. \tag{III}$$

here, Q_2 is the process heat of (II).

It is assumed that the compounds A_2, AM and XM do not exist. The composition of the gas is determined by the concentrations [AX], [A], [X], $[X_2]$ and [M]. They are interrelated by the relationships: [AX] + [A] = (ρ ρ_0 = $(\rho/\rho_0)[AX]_0$, [AX] + [X] + 2$[X_2]$ = $[(\rho/\rho_0)AX]_0$. Taking them into account, one can write the equations for any two concentrations, for example, for [AX] and [X]:

$$\frac{\partial}{\partial t}[AX] = -W_J + W_2 - W_3, \tag{5}$$

$$\frac{\partial}{\partial t}[X] = W_J - W_2 - W_1, \tag{6}$$

where $W_J = \sigma[AX]J$; W_i (i = 1, 2, 3) are the rates of the forward processes of (I) - (III). The quantities W_i have the form

$$W_1 = k_1[X]^2[M],\ W_2 = k_2[A][X][M],\ W_3 = k_3[AX][X], \tag{7}$$

where k_1-k_3 are the constants of the reactions rates for (I) - (III), which do not depend on T. The thermal balance equation is written in the conventional way. Thus, for the photolysis scheme of A, it has the form:

$$[M]Rc_M\frac{dT}{dt} = (\hbar\omega_L - Q_1)W_J + \frac{1}{2}Q_1W_1, \tag{8}$$

where Rc_M is the heat capacity of the diluent.

The equations cited here should be supplemented with the initial and boundary conditions. We shall assume that at the point in time t = 0, raditiation falls on the boundary of the medium x = 0 having a constant photon flux of J (x = 0,t) = J_0, t $\geq$ 0. For the points x < ct, the following intensity distribution is established by the point in t = x/c:

$$J(x, t) = J_0e^{-\varkappa_0 x},\quad \varkappa_0 \equiv \varkappa(t=0), \tag{9}$$

in which case, over these times, only an insignificant change in the concentrations of the original components occurs. A further substantial change in J and the other characteristics of the system occurs after significantly greater times (of photolysis and the chemical reactions). For this reason, the first term in equation (1) can be omitted, and the distribution of (9) is referenced to the point in time t = 0. The initial conditions for the chemical kinetics equations have the form:

For photolysis scheme A: $[X_2]=[X_2]_0$, $[X]=0$, $t=0$;

For photolysis scheme B: $[AX]=[AX_0]$, $[A]=[X]=[X_2]=0$, $t=0$.

We assume: $T(x,o) =T_0$, $\rho(x, 0)=\rho_0$, $v(x, 0)=0$, $v(0, t)=0$.

2. The Photolysis of Homonuclear Biatomic Molecules. The Linear Mode.

We shall begin the treatment of photolysis in accordance with scheme A with the simplest case, for which the medium is not bleached. In this case, the distribution of J(x, t) does not depend on t and is determined by formula (9). Neglecting gas dynamic perturbations (they are estimated below), we introduce the dimensionless parameters:

$$\zeta_1=[X]/2[X_2]_0,\ \zeta_2=[X_2]/[X_2]_0=1-\zeta_1,\ I(x)\equiv J(x)\,\sigma\, t_{рек},$$
$$t_{рек}=(4k_1[X_2]_0[M])^{-1},\ \tau=t/t_{рек},\ \theta=T/T_0,\ \eta\equiv[AX]_0/[M]. \tag{10}$$

[$t_{pek} = t_{rec}$]

Then we find ζ_1 in simple form from kinetics equations (3):

$$\zeta_1=\sqrt{I(x)}\,\mathrm{th}\left(\tau\sqrt{I(x)}\right). \tag{11}$$

for θ, we find from (8):

$$\frac{\partial\theta}{\partial\tau}=(A-B)I\zeta_2+B\zeta_1^2,\quad A\equiv\frac{\hbar\omega_L\eta}{Rc_MT_0},\quad B\equiv\frac{Q_1\eta}{c_MRT_0}. \tag{12}$$

Formulas (11) and (12) are justified in the absence of bleaching, i.e., for $\zeta_1 \ll 1$. This condition is met for any I if τ is small ($I\tau \ll 1$) and for all τ, if

$$I(0)\equiv I_0\ll 1. \tag{13}$$

An analysis of the inverted population criterion. We shall employ the inverted population criterion for the X_2 molecules, formed in the process

of recombination (I), which is given in [9]:

$$[X]^2 \geqslant [X_2]\, K_1(T)\, e^{\hbar\omega/kT}, \qquad (14)$$

where $K_1(T)$ is the chemical reaction equilibrium constant for I; ω is the frequency of the working photo transition. We shall assume that $K_1(T) = K^0 e^{-Q_1/RT}$. Using (11) and (12), this criterion is written in the form

$$I \operatorname{th}^2(\tau\sqrt{I}) > \varkappa^0 \exp\left\{-\frac{(1-\Omega)\,Q_1/RT_0}{1 + A/\tau - B\sqrt{I}\operatorname{th}(\tau\sqrt{I})}\right\}, \qquad (15)$$

where $\varkappa^0 \equiv K_1^{(0)}/(4\eta\,[M])$, $\Omega \equiv \hbar\omega/Q_1$. Formula (15), along with equation (9), solves the problem of determining the spatial regions with an inverted population and their timewise evolution. It is convenient to study (15) in explicit form in the plane I, τ. Our treatment is justified only for the portion of the plane adjacent to the axes $I = 0$ and $\tau = 0$, and bounded by the curve $\zeta_1(\tau, I) = 1$. We shall partition this portion of the plane by the line $\tau\sqrt{I} = 1$ (curve 1 in Figure 1a). An inverted population appears below this line in the region $\tau\sqrt{I} \ll 1$ under the condition $F(T_0, \Omega) \equiv K^0 \cdot \exp[-Q_1(1-\Omega)/RT_0] \ll 1$. The inversion curve, which separates the region where (15) is observed, proves to be a hyperbola: $I\tau = [F(T_0, \Omega)]^{1/2}$ (curve 2). It follows from (15) for the inversion curve in the region $1/(I)^{1/2} \ll \tau \ll 1/I$ that $I \simeq$ const. $= F(T_0, \Omega)$ (curve 3). The line $I\tau \simeq (Q_1/RT_0)(1-\Omega)/A \ln K^0$ (curve 4) is approximately obtained for $I\tau \gg 1$. The strait line $I = I_0$ is to be drawn for a specified incident radiation intensity I_0 in Figure 1a, since in the working volume $I \leq I_0$. Thus, the inversion region in the variables I and τ proves to be an island, the boundaries of which depend substantially on the temperature T_0: with an increase in T_0, the island is reduced and when $T_0 \geq (Q_1/I)(1-\Omega)/\ln(K^0/T_0)$ disappears. In this case, the intensity of the external light is insufficient to produce the inversion. For:

$$T_0 \geqslant \frac{Q_1(1-\Omega)/R}{\ln \varkappa^0} \qquad (16)$$

an inversion cannot form.

Using the results presented, it is not difficult to describe the behavior of an inversion in the space-time variables x and τ (Figure 1b). The most important conclusions from this treatment are the finite time of the existence of an inverted population at each of the points in space and the shift of the region in which the inversion is realized.

If criterion (14) is observed, then the light gain can be represented in the form:

$$\alpha = a(\omega, T)\,[X]^2, \qquad (17)$$

where $a(\omega, T)$ depends on the type of molecules and was computed for various cases in [5, 9 - 11]. It is easy to compute α using the formulas

given here. If a does not depend substantially on T, then α reaches a maximum in the region $\tau\sqrt{I} > 1$: $\alpha_{max} = 4aI[X_2]_0^2$. For the latter case, the qualitative course of the surves $\alpha(x, \tau) = \text{const}$ is shown in Figure 1b.

In conclusion, we shall give the expressions for gas dynamic perturbations of the density:

$$\frac{\rho-\rho_0}{\rho_0}=\frac{J_0c_MC}{[X_2]_0(1+c_Ma_0}\begin{cases} e^{-\varkappa_0 x}\,[\mathrm{sh}\,(t/t_p)-t/t_p], & x>a_0t \\ -\left[t/t_p\ e^{-\varkappa_0 x}+\mathrm{ch}\,(\varkappa_0 x)\,e^{-t/t_p}-1\right], & x<a_0t, \end{cases} \qquad (18)$$

where $t_p = (\kappa_0 a_0)^{-1}$; $C = A - B$. for $t_{rec} >> t_p$ and $C = A$ for $T_{rec} << T_p$; a_0 is the velocity of sound in the undisturbed gas. In actual cases, $J/([X_2]_0 a_0) \simeq A \simeq B \simeq 1$, and for this reason, it follows from (18) that the gas dynamic perturbation can be neglected only when $t << t_p$.

3. The photolysis of the X_2 molecules in a decaying bleaching wave.

We shall consider the photolysis of the mixture A at intensities such that bleaching effects occur:

$$I_0 \gg 1. \qquad (13')$$

We shall introduce the dimensionless variables $p \equiv \sigma \int_0^x dx\,[X_2]$ and $\chi \equiv x\sigma[X_2]_0/I_0$; then $J = J_0\exp(-p)$, and instead of (1) and (3), we find:

$$\frac{1}{I_0}\frac{\partial^2 p}{\partial\tau\,\partial\chi} = -\frac{\partial p}{\partial\chi}e^{-p}+\left(1-\frac{1}{I_0}\frac{\partial p}{\partial\chi}\right)^2. \qquad (19)$$

It is characteristic of (19), that the left side contains a small parameter in the case of the higher derivative. This term can be comparable with the other terms of (19) only in a narrow space-time zone, which separates the regions in which the solution depends continuously on χ and almost does not depend on τ. One of these regions corresponds to the initial medium where $\frac{1}{I_0}\frac{\partial p}{\partial\chi} \cong 1$. Continguous to it is the region of rapid change in p (the bleaching front), where instead of (19), one can write: $\frac{1}{I_0}\frac{\partial^2 p}{\partial\chi\,\partial\tau} = -\frac{\partial p}{\partial\chi}e^{-p}$, from which:

$$p = \ln\left\{\varphi(\tau)\left[e^{I_0\chi}+I_0\int_0^\tau d\tau'\varphi^{-1}(\tau')\right]\right\};$$
$$\zeta_2 = 1\Big/\left[1+I_0\,e^{-I_0\chi}\int_0^\tau d\tau'\varphi^{-1}(\tau')\right]. \qquad (20)$$

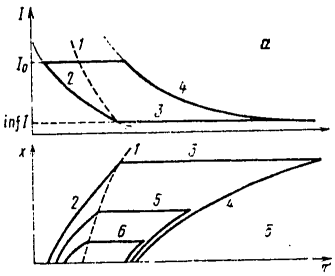

Figure 1. The inversion regions for the case of linear mode photolysis.

Sections 2, 3 and 4 of the inversion curve (a) correspond to lines 2, 3 and 4 of (b); curves 5 and 6 correspond to lines of constant gain, α (x, τ) = const.

The "fast solutions" (20) likewise make a transition to smooth functions from the side of small values of χ. In this region, we derive the equation $\frac{\partial p}{\partial \chi} e^{-p} = \left(1 - \frac{1}{I_0}\frac{\partial p}{\partial \chi}\right)^2$, from (19), where the solution of this equation has a simple form:

$$p = -\ln(1-\chi),\quad \zeta_2 = [I_0(1-\chi)]^{-1}. \qquad (21)$$

by tying (20) and (21) together at the point $\chi_\Phi(\tau)$ where all of the terms of equation (19) are of the same order of magnitude, we find $\phi(\tau)$, p, ζ_2 and the explicit form of $\chi_\Phi(\tau)$. We shall give ζ_2 and χ_Φ:

$$\zeta_2(\chi, \tau) = [1 + I_0 \exp\{-I_0(\chi - \chi_\Phi(\tau))\}]^{-1},$$

$$\chi \approx \chi_\Phi(\tau) = 1 - e^{-\tau}. \qquad (22)$$

The found solutions describe a nonsteady-state photodissociation wave, the amplitude and velocity D(t) of which fall off with time ($D = J_0 e^{-\tau}/[X_2]_0$). The characteristic decay time is about t_{rec}, and the depth of penetration into the working volume is $\chi \approx 1$ or $x \approx \kappa_0 I_0$, something which is I_0 times greater than the similar characteristic for the linear absorption mode.

The inverted population criteria. For the temperature in the photolysis front, we find from (12): $\phi = 1 + (1 - \zeta_2)(A - B)$. By substituting ϕ and $\zeta_1 = 1 - \zeta_2$ in (14), we find that if the following condition is met:

$$6c_M(1-\Omega) > \eta\left(\frac{\hbar\omega_L}{Q_1} - 1\right)(\ln \mathcal{K}^0)^2 \qquad (23)$$

or

$$T_0 < T_{0m} \equiv \frac{Q_1}{R}\left[\frac{1-\Omega}{\ln \mathcal{K}^0} - \frac{\eta}{c_M}\left(\frac{\hbar\omega_L}{Q_1} - 1\right)\right],$$

then an inverted population arises in the front and is maintained in a certain region of the bleached gas. It $T_0 > T_{0m}$ or $T_{0m} < 0$, then the inversion exists only in the photolysis wave front itself. When (16) is met, inversion does not occur.

Estimates show that for actual values of the gas parameters, a mode is realized where inversion occurs in the front while it is maintained

following the front of the bleaching wave. In the bleached region, we find from (12) and (21) that: $\theta \cong \theta_\Phi + A\,(\tau - \tau_\Phi(\chi))$; $\theta_\Phi = 1 + A - B$; ; $\tau_\Phi(\chi) = -\ln(1-\chi)$ is the moment the front passes through the point χ. This expression permits the determination of the time of existence of the inversion following the photolysis front in the bleached region:

$$R\,(T_{0m} - \tau_0)\, c_M/(\eta \hbar \omega_L) = \text{const}. \tag{24}$$

The conditions found here show that behind the bleaching wave front, a quasisteady-state "inversion wave" propagates through the gas. In the case considered here, the thickness of the inversion layer is smaller than at low intensities (13). However, the concentrations of the atoms achieve the greatest possible values $[X] = 2[X_2]_0$, while the light gain in the inversion layer is equal to $\alpha = 4a(\omega, T)\,[X_2]_0^2$.

The actual gas dynamic mode. Depending on the velocity of the photodissociation wave, various modes of gas motion are possible. The most interesting case is that of a fast wave, when a section of almost steady-state, quasihomogeneous gas flow exists behind the wave front (the light detonation mode). In equations (3), (5) and (6), $\partial/\partial t$ is to be replaced by d/dt, and the gas dynamics equations of [8] are to be written. It turns out that the photolysis wave velocity D(t) does not change, while the indicated quasisteady-state mode is possible when

$$d \equiv \frac{D(t)}{a_0} \geqslant d_1 = \sqrt{\frac{1+2c_M}{2(1+c_M)}L + 1} - \sqrt{\frac{1+2c_M}{2(1+c_M)}L}, \tag{25}$$

where $L = A - B$. Quasisteady-state flow is realized for $\chi' \leqslant \chi \leqslant \chi_\Phi$, where the lower boundary χ' is due to wave rarifaction, where the wave propagates at the local velocity of sound $\frac{d\chi'}{d\tau} = \frac{1}{d(0)}\sqrt{\theta(\chi', \tau)} + s$, $s \equiv v/a_0$ for the density, temperature and velocity, we find:

$$\frac{\rho_0}{\rho} = 1 - \frac{s}{d}, \quad \theta = \left(1 - \frac{s}{d}\right)(1 + \gamma(1 + 1/c_M)ds),$$
$$s = \frac{d^2 - 1 \pm \sqrt{(d^2-1)^2 - 2d^2L(1+2c_M)/(1+c_M)}}{(1+2c_M)\,d/c_M}. \tag{26}$$

Estimates show that the change in ϕ from (26) is the most important for the gain conditions. The light detonation front, bleaching wave, inversion layer and region of quasisteady-state flow are illustrated in Figures 2 and 3.

4. Photolysis of AX Molecules which Occurs According to the Scheme (I) - (III)

A type B mixture, when $t \to \infty$, as follows from equations (5) and (6), is completely bleached when subjected to radiation (in contrast to the A mixture), however, the bleaching, generally speaking, is not of a wave nature. The mode closest to the bleaching wave is realized only at the

limit supr(I_0, β') >> β, where $\beta \equiv k_2/k_1$, $\beta' \equiv k_3/k_1[M]$, when process (II) is suppressed (the inverse with respect to photodissociation). We shall consider only the case where the greatest concentrations of atoms are realized:

$$I_0 \gg \beta, \beta' \ (\beta \gtrsim 1). \tag{27}$$

With condition (27), just as in section 3, a narrow space-time region is successfully singled out (the wave front), in which the intensity falls from a certain value of I_Φ down to zero, almost AX dissociation occurs and the atoms are built up to concentrations of $[X] \approx [X]_{max} \equiv [AX]_0$. The front propagates with a velocity $D(t) = J_0 I_\Phi(t)/([AX]I_0)$. The value of I_Φ is determined by the residual absorption in the bleached region. Behind the wave front, we find for the concentration X:

$$[X] \cong [AX]_0/[1+\tau-\tau_\Phi(x)] \tag{28}$$

(for this section, $2[X_2]_0 \to [AX_0]$ should be substituted in the dimensionless parameters of (10) twice. Here $\tau_\Phi(x)$ is the moment the front passes through the point x; $I_\Phi(\tau)$ is determined by the equation:

$$I_\Phi(\tau) = I_0 - \beta \int_0^\tau d\tau' \frac{I_\Phi(\tau')}{1+\tau-\tau'}. \tag{29}$$

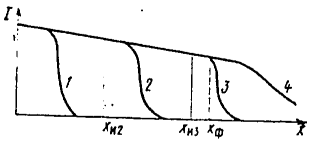

Figure 2. A nonsteady-state photodissociation wave.

Curves 1-3 correspond to the points in time $t_1 < t_2 < t_3$; 4 corresponds to a steady-state distribution, which is realized when $t \to \infty$; x_{M2} and x_{M3} are the coordinates of the end of inversion for the points in time t_2 and t_3.

We shall give the solutions of this equation in two limiting cases:

$$\beta \gtrless 1. \tag{30}$$

The upper condition corresponds to the maximum transition to a type A mixture, and for this reason, the result $I_\Phi = I_0 e^{-\beta\tau}$ for $\beta\tau \lesssim 1$ agrees with the formulas of section 3 within a precision of the symbols $k_1 \to k_2$. For the lower inequality of (30), we find from perturbation theory that

$I_\Phi - I_0 \simeq \beta \ln(1 + \tau)$, i.e., for the times

$$\tau < e^{1/\beta} - 1 \tag{31}$$

$I_\Phi \simeq I_0$. The depth of penetration of the photolysis wave into the gas is equal to about $\kappa_0^{-1} I_0 e^{1/\beta}$, greater than for an A mixture.

For the temperature in the wave front, we find $\theta = 1 + (A - B_1)\zeta_1$, and behind the wave front:

$$\theta(\chi, \tau) = 1 + (A - B_1) + A\beta \ln [1 + \tau - \tau_\Phi(\chi)] + (B_1 + B_2)(\tau - \tau_\Phi)/(1 + \tau - \tau_\Phi), \tag{32}$$

where

$$B_1 = Q_2\eta/(c_M R T_0); \quad B_2 = (1/2 Q_1 - Q_2)\eta/(c_M R T_0).$$

Here, the second term corresponds to the liberation of energy with the residual absorption of light, and the third is for the recombination case.

The output of products can be determined from equations (5) and (6). Immediately behind the wave front, we obtain the following with logarithmic precision $[X_2] = [AX] \cdot \ln[I_0/2I_\Phi(\tau)$, and later, $[X_2] \simeq ([AX]_0 - [X]/2)$, where [X] is to be taken from (28). Using these results, it is to calculate the inversion criteria (14). We shall give the condition for maintaining the inversion behind wave fronts in a recombining gas:

$$T_0 \leqslant \frac{Q_1}{R}\left\{\frac{1-\Omega}{\ln(\mathcal{H}^0 \ln I_0/I_\Phi)} - \eta\frac{\hbar\omega_L - Q_2}{c_M Q_1}\right\}. \tag{33}$$

Just as above, we are citing formulas which take into account gas motion, only for the case where a region of quasisteady-state gas flow exists behind the photolysis wave front. This case is realized when $D(t) > a_0 d_1$, where d_1 is determined by (25) with $L = L_1 = A + B_2$; the change in the other parameters behind the wave front is determined by the formulas of (26), in which we are to assume that $L = A + B_2 - (B_1 + B_2)\zeta_1$, and $2[X_2] = (\rho/\rho_0)[AX]_0 - [X]$. The following inexplicit expression is obtained for [X] as a function of τ and χ:

$$\int_{\zeta_1}^{1} d\zeta_1 \left(\frac{\rho_0}{\rho}\right)^2 \frac{1}{\zeta_1^2} = -(\tau - \tau_\Phi(\chi)).$$

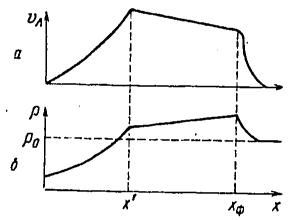

Figure 3. The velocity (a) and depth (b) of the gas as a function of the coordinate in the rarefaction waves $0 < x < x'$, in the region of quasisteady-state flow $x' < x < x_\Phi$ and in the bleaching front $x = x_\Phi$ for $t = t_3$ (see Figure 2).

These formulas completely define ρ, v, θ, [X] and [X_2] behind a photolysis wave front, taking gas motion into account; they can be used to compute the inversion criteria (14) and the light gain.

5. Specific Substances which Are Suitable for an Optically Pumped Recombination Laser

We used published data on the spectral photodissociation regions to calculate the photolysis of specific mixtures: $\lambda_1 - \lambda_2$; the mean values of the photodissociation cross-sections in these ranges of σ; the values of the reaction rate constants k_1. The values of J_0 were computed for the indicated spectral ranges for a source with a high brightness temperature of $T_b = 4 \cdot 10^4$ K. All of these quantities are given in Tables 1 and 2. Also shown there are the functions a(T) which we computed (see(17)). The values of the reaction heat and chemical equilibrium constants were taken from [12]. In all cases (with the exception of the gas S_2), $T_0 = 300°$ K.

Photolysis of the gas Cl_2. We shall consider a mixture of Cl_2-N_2 where $[Cl_2]_0 = 5 \cdot 10^{18}$ cm^{-3} and $\eta = 0.3$. For the parameters of Table 1, $\kappa_0^{-1} = 0.5°$ cm, $t_{rec} = 2$ microseconds, $I_0 = 0.12$ (see (10)), i.e., the linear photolysis mode is realized (section 2). The inversion formation criterion (16) has the form $T_0 < T_{max} = 1{,}130°$ K and is easily met. The gas parameters depend on x. We shall consider them for $x = \kappa_0^{-1}$. The inversion existence time at this point is $\Delta\tau_1 = 6.9$ ($\Delta t_1 = 13$ microseconds). At the moment of inversion disruption, the gas is heated up to $T = T_{max}$, and [Cl] = $7 \cdot 10^{18}$ cm^{-3}. We shall give the photolysis parameters for one of the points in time for which the inversion is realized: $\tau = 3.5$. We find from (11) and (17) that [Cl] = $2.6 \cdot 10^{18}$ cm^{-3} and T = 640° K. The change in the density due to gas dynamic perturbations is $(\rho - \rho_0)/\rho_0 =$ = 0.09 (see (18)). The light gain is $\alpha = 4.3 \cdot 10^{-3}$ cm^{-1}. Thus, for the case of Cl_2 photolysis in layers of about 0.5 cm for a duration of $\simeq$ 10 microseconds, a gain is realized which exceeds 10^{-3} cm^{-1}.

The photolysis of Br_2 *gas.* We shall consider a mixture of Br_2-Co_2 at [Br_2] = 10^{18} cm^{-3} and $\eta = 0.25$. For the parameters of Table 1, we find $t_{rec} = 6$ microseconds, $\kappa_0^{-1} = 2.2$ cm and $I_0 = 8$. A photodissociation wave is realized having a velocity $D_0 = 2$ km/sec ($d_0 = 14$), the limiting velocity is $d_1 = 2.7$ (see (25)), so that the quasisteady-state flow region behind the front exists for $x \leq 14$ cm, while the total depth of wave penetration into the volume amounts to 17 cm. The temperature behind the front is 740° K. It follows from (23) that inversion is realized only in the wave front. We shall give the gas parameters at the point in time $\tau = 0.7$, when the front is located at the point x = 9 cm, I = 4. The gas behind the front is accelerated up to velocities of 40 m/sec, and in the front, [Br] = $1.5 \cdot 10^{18}$ cm^{-3}; using (17), we find the mean gain in the front: $\alpha = 2.4 \cdot 10^{-4}$ cm^{-1} and $\lambda = 1{,}320$ nm.

TABLE 1

Substance / Вещество	σ, см²	Δλ, нм nm	1. J_0, фот/(см².с)	2. $k_1 \cdot 10^{33}$, см⁶/с ($T \approx 1000$ K)	3. Q_3, ккал/моль	$a(\lambda, T)$, см²
Cl_2	$1{,}9 \cdot 10^{-19}$ [14]	285—375 [14]	$3{,}4 \cdot 10^{23}$	0,4 [15]	57 [12]	$\left.\begin{matrix}1{,}8 \cdot 10^{-42} \\ 0{,}8 \cdot 10^{-43}*)\end{matrix}\right\} \times \times \left(\frac{1000}{T}\right)^{3/2} \exp\left(\frac{3360}{T}\right)$ $\lambda = 1200$ нм nm
Br_2	$4{,}5 \cdot 10^{-19}$ [14]	370—520 [14]	$3 \cdot 10^{23}$	0,8 [15]	45 [21]	$\left.\begin{matrix}7 \cdot 10^{-43} \\ 7 \cdot 10^{-44}*)\end{matrix}\right\} \times \times \left(\frac{1000}{T}\right)^{3/2} \exp\left(\frac{3150}{T}\right)$ $\lambda = 1320$ нм nm
S_2	$1{,}5 \cdot 10^{-17}$ [16]***)	240—290 [16]	$2{,}4 \cdot 10^{23}$	2,8[17]**)	100 [21]	$\left.\begin{matrix}7 \cdot 10^{-41} \\ 1{,}5 \cdot 10^{-41}*)\end{matrix}\right\} \times \times \left(\frac{1000}{T}\right)^{3/2} \exp\left(\frac{3,900}{T}\right)$ $\lambda = 450$ нм nm

Key: 1. J_0, phot/(cm^2 . sec);
2. $k_1 \cdot 10^{33}$, cm^6/sec ($T \approx 1{,}000°$ K);
3. Q_3, Kcal/mole;

*) The value of $a(\lambda, T)$ is given for high pressures in the gas, when the rotational structure in the radiation spectrum disappears. In other cases, the value of $a(\lambda, T)$ corresponds to the doppler widening of the electron-vibrational-rotational line and to the transition with the maximally populated rotational level.

**) The measured value in [17] amounts to 27% of the total recombination constant k_1 where T = 300° K [11]. A temperature dependence of $k_1 \approx 1{,}000°$ K/T was adopted.

***) The mean value for the indicated band is given, which corresponds to transitions at the level $v' \approx 10 - 26$ $S_3(B^3\Sigma_u^-)$, which effectively decays as a result of spontaneous and induced predissociation collisions [14].

The photolysis of S_2 gas. We shall consider a mixture of S_2-N_2 at $T_0 = 700°$ K, when a concentration of $[S_2]_0 = 10^{18}$ cm^{-3} is achieved. From Table 1, when $\eta = 0.25$ we find that $t_{rec} = 22$ microseconds, $\kappa_0^{-1} = 0.07$ cm

and $I_0 = 80$. A bleaching wave with a velocity of 4.7 km/sec is realized ($d_0 = 5.2$, and the limiting velocity of (25) is equal to 1.8). The total penetration of the wave into the gas is 5.3 cm, and quasisteady-state flow behind the wave front is possible when $x < 4$ cm. We shall consider the state of the gas when $\tau = 0.9$: the front is located at $x = 3.2$ cm, and $I = 32$; the extent of the nonsteady-state flow is 1.6 cm; behind the front, the gas is accelerated up to $v = 0.13$ km/sec; $T = 1{,}060°$ K; the compression is $\rho/\rho_0 = 1.15$; the concentrations are $\zeta_1 \approx 1$ and $\xi \approx 0.03$. For $\lambda = 450$ nm, the inversion layer amounts to about 0.16 cm; inversion is disrupted when $T = 1{,}500°$ K. The gain right behind the front is equal to $1.2 \cdot 10^{-2}$ cm^{-1} and at the moment inversion is broken off, $4 \cdot 10^{-3}$ cm^{-1}. For $\lambda = 550$ nm, the inversion layer is about 0.66 mm, inversion is lost at $T = 2{,}000°$ K and the gain behind the front is $3 \cdot 10^{-3}$ cm, while at the moment of inversion loss, it is $4.6 \cdot 10^{-4}$ cm^{-1}.

It can be seen that the levels of the gain are sufficient to realize generation or recombination pumping. We will note that in [13], an S_2 laser was optically pumped with direct optical excitation of the upper lasing state of S_2 (B).

Photolysis of COS gas. In the photolysis of COS, sulfur atoms in the $^1D_2$ and $^1S_0$ excited states are formed in the spectral range indicated in Table 2. We shall consider those pressures at which these states are deactivated before the exchange chemical process of type (III) occurs. We shall consider a gaseous mixture of COS-CO_2, where $[COS] = 2 \cdot 10^{18}$ cm^{-3} and $\eta = 0.05$. Using Table 2, we find $t_{rec}^{(I)} = 5$ microseconds, $\kappa_0^{-1} = 0.04$ cm; $I_0 = 28$, $\beta = 0.05$ and $\beta' = 0.1$ (an exchange constant of $k_3 = 1.3 \cdot 10^{-14}$ cm^3/sec was used). The conditions of (27) are met, i.e., maximum concentrations of $[S] = 2 \cdot 10^{18}$ cm^{-3} are achieved in the wave front; the layer in which the recombination occurs is 1 cm thick. The wave penetration depth is practically unlimited. Condition (29) leads to the criterion for the occurrance of inversion, $T_0 < 1{,}320°$ K for $\lambda = 550$ nm. Right behind the wave front, $T = 760°$ K, and as a result of establishing chemical equilibrium, $T = 1{,}020°$ K is established, i.e., the inversion is preserved right up to the complete recombination of the S atoms. The maximum gain of $\alpha = 10\text{-}3$ cm^{-1} is realized immediately behind the wave front at the point where half of all the atoms has reacted, $\alpha = 2 \cdot 10^{-4}$ cm^{-1}.

Thus, the photolysis of COS can be accomplished practically any depth of the gas, the inverted population at the S_2 (B → X) transition is preserved in the extended layers of the gas and a gain is achieved which is sufficient to excite lasing.

Photolysis of CH_3Br gas. In the case of photodissociation of CH_3Br, the following reactions occur: $CH_3Br + \hbar\omega_L \rightarrow CH_3 + Br$, $CH_3 + Br \rightarrow CH_3Br$ (II), $2CH_3 \rightarrow C_2H_6$ (I), $Br + Br + (M) \rightarrow Br_2 + (M)$ (I'). As compared to photolysis scheme B. this process has two recombination channels, I and I', in which case, both reactions promote bleaching of the medium. Exchange

reactions III are slow because of the energy barrier. Reactions II and I are two-frequency reactions and occur at greater rates, and process I' is significantly lower, and for this reason, the results of section 4 can be applied to the entire process, if we set A ≡ Br and X ≡ CH_3 everywhere (with the exception of the inversion criteria).

TABLE 2

A—X	λ, nm [1,14]	σ, см²	$J_0 \cdot 10^{-23}$, фот/(см²·с)	k_1, cm^6/sec	Q_1, ккал/моль [12]
			phot./(cm^2·s)		Kcal/mole
CO_2	105—115	$1{,}5 \cdot 10^{-17}$ [14]	2	$1{,}7 \cdot 10^{-34}$ [18]	127
COS	140—180	$1{,}5 \cdot 10^{-17}$ [1]	4,3	$2 \cdot 10^{-34}$*)	72
CH_3Br	140—260	$7 \cdot 10^{-19}$ [14]	10	$4{,}7 \cdot 10^{-11}$**) 10^{-12}***)	67

*) The calculation is based on the decay rate constant from [19] and the chemical equilibrium constant of [12].

**) The dual frequency reaction rate constant of $CH_3 + CH_3 \rightarrow C_2H_6$ [cm^3/sec] [18].

***) The same, for $CH_3 + Br \rightarrow CH_3Br$.

By way of example, we shall consider the mixture CH_3Br-CO_2 with a concentration of $[CH_3Br] = 4 \cdot 10^{18}$ cm^{-3} and $\eta = 0.04$. For the parameters of Table 2, we find $D_0 = 2.5$ km/sec, $t^I_{rec} = 5$ ns and $t^{I'}_{rec} = 3$ microseconds. The Br atoms recombine over a length of $l^I_{rec} = 0.8$ cm, the temperature behind the bleaching front is 700° K, and following recombination of the Br atoms, it is 780° K. The inversion criterion is met right up to the complete disappearance of the Br atoms, and the gain is $\alpha_{max} = 1.2 \cdot 10^{-4}$ cm^{-1}.

6. Conclusion

We shall summarize the major results and conclusion of the paper. The photolysis of gaseous media has been studied, in which some of the major chemical processes are recombination reactions. It is shown that with the action of high power radiation, these media are completely or partially bleached in nonsteady-state photochemical waves. At the maximum intensity, a theory has been constructed for such waves. It is shown that a case exists, of the greatest interest for lasers, for which quasisteady-state flow, having the greatest homogeneity, is realized behind the photolysis wave front. Intense radition can produce large concentrations of atoms and radicals (10^{18} - 10^{19} cm^{-3}) and initiates strongly nonequilibrium recombination reactions. An inverted population of molecules--recombination

products was studied. Inversion can occur both with linear absorption of light and in bleaching modes. The degree of dilution of the working gas has a substantial influence on the inversion criteria.

The theory developed was used to calculate the photochemical wave, gas dynamic parameters and inverted population which arise during the photolysis of specific mixtures, for which the effective population of the excited molecular states in the recombination reaction are well known from the literature. The optical pumping conditions, under which recombination laser operation is possible, are determined. The optical pumping of the lasers treated here is of the greatest interest, since considerable excited particle densities should be achieved in them; large working volumes can be used, and the broad dissociation spectra permit the efficient utilization of the pumping energy. Optical pumping can also serve as a simple approbation of the recombination mechanism of laser excitation, which can also be realized under other ("dark") conditions and are promising for applications in high power flow type chemical lasers using electron phototransitions [5, 20-22].

BIBLIOGRAPHY

1. L.D. Mikheyev, KVANTOVAYA ELEKTRONIKA [QUANTUM ELECTRONICS], 5, 1189 (1978).

2. V.S. Zuyev, S.B. Kormer, L.D. Mikheyev, M.V. Sinitsyn, I.I. Sobel'man, G.N. Startsev, PIS'MA V ZHETF [LETTERS TO THE JOURNAL OF EXPERIMENTAL AND THEORETICAL PHYSICS], 16, 222, (1975).

3. V.S. Zuyuv, L.D. Mikheyev, V.I. Yalovoy, KVANTOVAYA ELEKTRONIKA, 2, 799, (1975).

4. V.A. Kochelap, "Kandidatskaya dissertatsiya" ["Candidate Degree Dissertation"], IP AN USSR [Institute of Semiconductors of the Ukrainian Academy of Sciences], Kiev, 1970.

5. A.S. Bashkin, V.I. Igoshin, A.I. Nikitin, A.N. Orayevskiy, "Khimicheskiye lazery. Itogi nauki i tekhniki. Ser. Radiotekhnika" ["Chemical Lasers. Progress in Science and Engineering. Radio Engineering Series"], Vol. 8, Moscow, VINITI AN SSSR [All-Union Institute of Scientific and Technical Information of the USSR Academy of Sciences], 1975, p 315.

6. V.Ye. Khartsev, ZhETF [JOURNAL OF EXPERIMENTAL AND THEORETICAL PHYSICS], 54, 856 (1968).

7. B.L. Borovich, V.S. Zuyev, O.N. Krokhin, ZhETF, 64, 1184 (1973).

8. L.D. Landau, Ye.M. Lifshits, "Mekhanika sploshnykh sred" ["The Mechanics of Continuous Media"], Moscow, GTTI Publishers, 1953.

9. V.A. Kochelap, Yu.A. Kukibnyy, S.I. Pekar, KVANTOVAYA ELEKTRONIKA, 1, 279 (1974).

10. A.I. Izmaylov, V.A. Kochelap, Yu.A. Kukibnyy, UKR. FIZ. ZHURNAL [UKRAINIAN JOURNAL OF PHYSICS], 21, 508 (1976).

11. A.S. Bashkin, N.L. Kupriyanov, A.N. Orayevskiy, KVANTOVAYA ELEKTRONIKA, 5, 421 (1978).

12. V.M. Glushko, "Termodinamicheskiye svoystva individual'nykh veshchestv" ["The Thermodynamic Properties of Individual Substances"], Moscow, USSR Academy of Sciences Publishers, 1962, Vol 2.

13. S.R. Leone, K.G. Kosnik, APPL. PHYS. LETTS., 30, 346, 1977.

14. J. Calvert, J. Pitts, "Photokhimiya" ["Photochemistry"], Moscow, Mir Publishers, 1968.

15. B.P. Levitt, "Fizicheskaya khimiya bystrykh reaktsiy" ["The Physical Chemistry of Fast Reactions"], Moscow, Mir Publishers, 1976.

16. L.A. Kuznetsova, N.Ye. Kuz'menko, Yu.Ya. Kuzyakov, Yu.A. Plastinin, UFN [PROGRESS IN THE PHYSICAL SCIENCES], 113, 19 (1974).

17. B.A. Thrush, R.W. Fair, DISC. FARADAY SOC., 44, 237 (1967).

18. B.N. Kondrat'yev, "Konstanty skorosti gazofaznykh reaktsiy" ["Gas Phase Reaction Rate Constants"], Moscow, Nauka Publishers, 1971.

19. A.J. Hay, R.L. Belford, J. CHEM. PHYS., 47, 3944 (1967).

20. B.A. Kochelap, Yu.A. Kukibnyy, KVANTOVAYA ELEKTRONIKA, 2, 1471 (1975).

21. V.A. Kochelap, Yu.A. Kukibnyy, IZV. AN SSSR. SER. MEKHANIKA ZHIDKOSTI I GAZA [PROCEEDINGS OF THE USSR ACADEMY OF SCIENCES. GAS AND FLUID MECHANICS SERIES], No 3, 174 (1977).

22. I.A. Izmaylov, V.A. Kochelap, Yu.A. Kukibnyy, S.I. Pekar, DAN SSSR [REPORTS OF THE USSR ACADEMY OF SCIENCES], 241, 80 (1978).

8225
CSO: 1862

LASERS AND MASERS

UDC 621.378.9

THE EFFECT OF THERMAL CHOKING SUPPRESSION WITH THE RESONANCE INTERACTION BETWEEN HIGH POWER LASER RADIATION AND A GAS FLOW

Moscow KVANTOVAYA ELEKTRONIKA in Russian Vol 6 No 11, 1979 manuscript received 23 May 79 pp 2476-2481

[Article by A.A. Stepanov and V.A. Shcheglov, Physics Institute imeni P.N. Lebedev of the USSR Academy of Sciences, Moscow]

[Text] The phenomenon of thermal choking in a supersonic flow of a chemically reacting gaseous mixture is analyzed. The conditions are found under which the choking situation knowingly does not arise. The possibility of laser control of gas dynamic processes in such flows is demonstrated, which permits suppression of the thermal choking under specific conditions.

1. It is well known (for example, see [1, 2]), that when heat is fed to a supersonic or subsonic flow, the flow velocity in a constant cross-section channel will fall off (or increase) until a critical value is reached, v_{cr} (the Mach number is M = 1), after which, further forced heat input proves to be impossible without changing the nature of the flow (the thermal choking phenomenon). Supercritical heat input can lead either to rearrangement of the steady-state flow (for example, to the formation of shock waves), or to the appearance of a nonsteady-state mode (in particular, surging).

2. In a typical situation, the heat source is a chemical reaction between a fuel and an appropriate oxidizer, or a discharge in the gas flow. It is not difficult to establish the criteria under which thermal choking knowingly begins in the system. For this, we make use of the conventional relationships which describe the gas flow in a cylindrical channel with heat input:

$$\frac{dT}{T}=\frac{1-\gamma M^2}{1-M^2}\frac{dQ}{H};\quad \frac{dM^2}{M^2}=\frac{1+\gamma M^2}{1-M^2}\frac{dQ}{H}, \tag{1}$$

where T is the temperature; γ is the adiabatic constant; Q is the heat supplied and H is enthalpy.

Simple calculations make it possible to determine the relationship between the heat input and the Mach number from (1):

$$\frac{Q}{c_p T_0} = \frac{1}{2}\left(1 - \frac{M^2}{M_0^2}\right)\left(\frac{1+\gamma M_0^2}{1+\gamma M^2}\right)\left(\frac{M^2-1}{1+\gamma M^2} + \frac{M_0^2-1}{1+\gamma M_0^2}\right), \tag{2}$$

where M_0 and T_0 are the initial parameters of the flow; c_p is the heat capacity for the case of constant pressure. We will note that in contrast to the estimating relationships given in [3], expression (2) is precise.

Setting M = 1 in (2), we obtain the maximum amount of heat, which corresponds to critical heating:

$$Q_* = c_0 T_0 (M_0 - M_0^{-1})^2, \tag{3}$$

where

$$c_0 = c_p/2(\gamma+1) = \gamma c_V/2(\gamma+1).$$

Taking (3) into account, the criterion for the occurrence of thermal choking is written in the form:

$$(c_0 T_0/Q)\,(M_0 - M_0^{-1})^2 < 1, \tag{4}$$

i.e., the choking situation is knowingly realized if the amount of heat Q delivered to the flow exceeds the critical value Q_*.

3. In this paper, attention is devoted to the fact that resonance interaction of laser radiation with the molecules of a gas flow which is heated by a chemical reaction, can, under certain conditions, have a substanital influence on the gas dynamic picture as a whole. In particular, this influence will act on the rate of change in the gas dynamic parameters along the flow as well as on their absolute values; in a number of cases, the radiation can remove the thermal choking effect, thus, the issue here is one of the possibility of laser control of gas dynamic processes in chemically active flows.

The analysis applies to the situation where the combustion reaction is accompanied by the formation of vibrationally excited molecules (reaction products). If the gas flow in which the vibrationally excited molecules are produced interacts with resonance laser radiation, then a definite portion of the amount of chemical energy will change into light energy through the channel coupled to the excited vibrational mode.

Radiation can be produced in a flow either by an external source (the amplification mode), or stimulated in the most active medium by passing this flow through a resonator (the generation mode). It is apparent that in this situation, the laser radiation will play the part of a "refrigerator.".

In a number of cases, even when condition (4) has been met, the thermal choking effect will not occur. The necessary and sufficient condition for the suppression of thermal choking in this situation is written in the form:

$$Q(1-\eta_x)<c_0T_0(M_0-M_0^{-1})^2, \tag{5}$$

where η_x is the efficiency of the conversion of the chemical energy to coherent radiation energy.

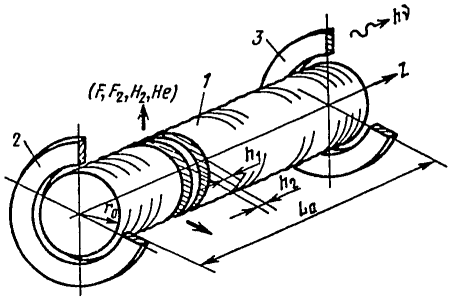

Figure 1. Simplified schematic of a CW ring model HF laser.

Key: 1. Cylindrical nozzle unit;
2,3. Resonator reflectors.

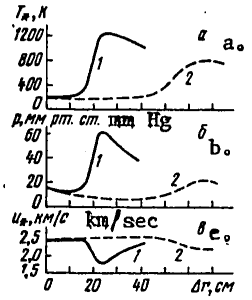

Figure 2. The distribution of the gas dynamic parameters averaged over the period of the structure, in a CW chemical HF laser with a cylindrical nozzle unit where $r_0 = 20$ cm and $\beta_{He} = 15$ ($\Delta r = r-r_0$).

Key: 1. Without a resonator;
2. In the generation mode.

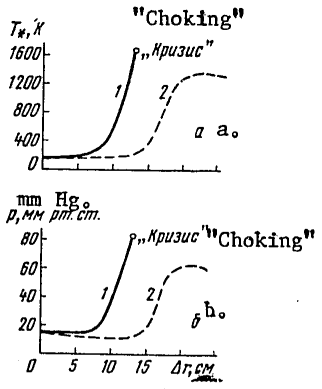

Figure 3. Illustration of the effect of thermal choking suppression in a supersonic flow by high power laser radiation (r_0 = 1.5 cm and β_{He} = 10).

Key: 1. Without a resonator;
2. In the generation mode.

4. The clearest influence of a resonance laser field on the gas dynamic picture of the flow should be manifest in the case of a chain reaction with a high energy yield for the case of the simultaneous radial expansion of the supersonic flow. The fact is that in this situation, combination action on the flow is accomplished by two factors immediately: radiation and geometric factors. Both factors permit the cooling of the gas flow, so that the criterion for the suppression of the thermal choking becomes less stringent as compared (5) [3].

By way of example, we shall conisder the supersonic flow of a working gas in a ring model of an HF laser with a chain excitation mechanism [3, 4]. The latter consists of a large number of coaxial annular nozzles with alternating jets of hydrogen and partially dissociated fluorine, diluted with helium (Figure 1). In step with the radial outflow, the streams are mixed, and in the mixing region, vibrationally excited HF (v) molecules are formed, which occur in the course of the chain reaction:

$$F+H_2 \rightarrow HF(v)+H+Q_1,\ Q_1=31{,}7 \text{ ккал/моль},$$
$$H+F_2 \rightarrow HF(v)+F+Q_2,\ Q_2=98 \text{ ккал/моль}.$$

The radiation propogates parallel to the axis of the cylinder inside the resonator, formed by ring shaped reflectors, and is of a tubular nature (the generation mode is being considered).

The effects studied here were analyzed on the basis of two-dimensional Navier-Stokes equations (in a boundary layer approximation), supplemented with equations of chemical, vibrational and radiation kinetics (for more details, see [3, 4]). The radius r_0 and the height L_a of the cylindrical nozzle unit was fixed in the calculations, as well as the ratio of the heights of the elementary nozzles h_1/h_2, the half-period of the structure of the nozzle block $h_* = (1/2)(h_1 + h_2)$, the reflection coefficients of the resonator reflectors r_1 and r_2 and also the original parameters of the oxidizer and fuel flows: the velocity u_{0i}, the temperature T_{0i}, the pressure p_{0i}, the degree of dilution of the oxidizer flow by the helium $\beta_{He} = [He]/([F_2] + (1/2)[F])$ ($i = 1, 2$; the subscript "1" applies to the oxidizer flow and "2" applies to the fuel flow). The following were adopted in a typical variant: $L_a = 1$ m, $h_1/h_2 = 2$, $h_* = 0.25$ cm, $r_1 = 0.98$, $r_2 = 0.9$, $u_1 = u_2 = 2.5$ km/sec, $T_1 = T_2 = 150°$ K, $p_1 = p_2 = 15$ mm Hg; the original degree of dissociation of the fluorine was assumed to be $\alpha_F = [F]/(2[F_2] + [F]) = 0.15$.

Characteristic results of the calculations are shown in Figures 2 and 3. Figure 2 illustrates the influence of the radiation field on the nature of the distribution of the gas dynamic parameters along the flow in the mode where the thermal choking effect does not occur (there is rather great dilution of the mixture with helium), however, the thermal effect in the medium are still rather substantial. In this case, the radiation field, in taking over a definite portion of the energy of the flow, by virtue of reducing the gas temperature leads to a considerable drawing out of the

developmental process of the chain reaction in the initial stage. A consequence of this is the enormously smoother change in the gas dynamic parameters in the presence of a radiation field than in the case where a resonator is absent.

The effect of thermal choking suppression in a supersonic flow by high power laser radiation is clearly demonstrated in Figure 3. It can be seen, that under the conditions considered here (weaker dilution of the mixture with helium than in the preceding case), in the absence of radiation, choking of the flow ($M \to 1$) occurs at a certain distance from the surface of the nozzle unit. If in a similar situation, a resonator is placed after the nozzle unit, then as the same calculations show, the choking can be removed in the generation mode by virtue of changing a portion of the chemical energy to radiation field energy. We will note that the radiation densities necessary for this are rather high, something which is due to the necessity of suppressing the channel for fast collision deactivation of the HF molecules, and this is possible only at intensities of $I > I_H$. Thus, in the case considered here, the saturation intensity close to the choking section amounts to $I_H \approx 10$ KW/cm^2, and in this case, radiation intensities of $I \approx 10^2$ KW/cm^2 are developed in the active medium of an HF laser.

BIBLIOGRAPHY

1. G.N. Abramovich, "Prikladnaya gazovaya dinamika" ["Applied Gas Dynamics"], Moscow, Nauka Publishers, 1976.

2. L.I. Sedov, "Mekhanika sploshnykh sred" ["Mechanics of Continuous Media"], Moscow, Nauka Publishers, 1970, Vol 2.

3. A.A. Stepanov, V.A. Shcheglov, "Preprint FIAN" ["Preprint of the Institute of Physics imeni P.N. Lebedev of the USSR Academy of Sciences"], Moscow, 1978, No 269; KVANTOVAYA ELEKTRONIKA, 6, 1476 (1979).

4. A.A. Stepanov, V.A. Shcheglov, "Preprint FIAN", Moscow, 1976, No. 182.

8225
CSO: 1862

NUCLEAR PHYSICS

UDC 538.121.8

INTERACTION OF A HIGH-INTENSITY RELATIVISTIC ELECTRON BEAM WITH MATTER

Moscow ATOMNAYA ENERGIYA in Russian Vol 47 No 5,1979 manuscript received 20 Nov 78 pp 328-332

[Article by A. N. Didenko, S. A. Chistyakov and A. P. Yalovets]

[Text] The results of numerical investigation of the interaction of a high-intensity electron beam with matter are presented. It is shown that energy transfer to the target material by the electron beam, besides inelastic collisions, is accomplished by means of conversion of coulomb energy of fast electron interaction with the field to thermal energy with resorption of the space charge which creates this field. The investigation showed that an increase of the incident current density with fixed value of conductivity of the medium leads to redistribution of the energy lost in the matter and an attempt was made to explain the effect of the abnormal energy absorption in thin oils during passage of a high-intensity electron beam through them.

Experimental data on the interaction of high-intensity electron beams (SEP) with matter, now published, indicate a difference of behavior in the SEP matter and ordinary (nonintensive) beams in some cases. Thus, abnormally high energy absorption in thin gold foil upon exposure of it to a powerful relativistic electron flux is indicated in [1] and a decrease in the depth of electron penetration into matter upon impingement of an SEP on it is noted in [2].

It is obvious that the corresponding theoretical investigations are required to understand the experimental results obtained and also for practical use of SEP. Because of the complexity of the problem of SEP interaction with matter, complete solution of it has not yet been possible. The simplest is the problem of finding a fast electron flux in matter upon impingement of an SEP on it. Solution of this problem permits one to find the main principles of SEP behavior in matter. It is this approach that is realized in this paper.

The system of equations and solution of it. Let us write a system of equations which describes the passage of an SEP through a layer of matter with surface coordinates z_0 and z_1. The short dissipation time of the fast electron energy in the condensed medium ($\tau_e \approx 10^{-12}$-10^{-11} s) permits one to write steady-state equations since τ_e is much less than the time which characterizes variation of the parameters of the beam impinging on the matter (variation of the current and energy of the SEP occurs during units and tens of nanoseconds). Moreover, a low value of τ_e also permits one to disregard variation of the state of matter related to the effect of the SEP on it. Hence, it follows that as a whole the nonstationary problem of SEP passage through the matter can be solved by sequential solution of steady-state problems at small time intervals. The case of one-dimensional configuration is considered, which is valid for beams whose transverse dimensions exceed the electron travel time in the matter.

When an SEP passes through matter, the relativistic beams, besides elastic and inelastic collisions with the atoms of the matter, interact with the electric field E, which in the general case is created by the space charge of the beam itself, the electrons and ions formed as a result of ionization of the medium and by thermalized electrons. In the steady-state case, the space charge of the beam is neutralized within time of approximately σ^{-1}, where σ is the conductivity of the medium, while the space charge created by the electron-ion pairs can be set equal to zero since secondary electrons are generated mainly with low energy and are thermalized near the point of their generation. Therefore, an electric field is created in the conducting medium by the space charge which is formed due to thermalization of fast electrons and is a source of conduction current.

Assuming that conduction of the medium in this case is such that resorption of the space charge occurs mainly due to conduction current, from the continuity equation for a charge, one can find an equation for the field which in one-dimensional configuration has the form

$$d(\sigma E)/dz = eN(z), \tag{1}$$

where e is the electron charge and N(z) is the rate of fast electron thermalization in plane z.

Since the field has a single component $E\{0, 0, E(z)\}$ in the considered configuration, the kinetic equation for the differential flux $\Psi(z, u, T)$ has the form [3]

$$L\Psi + EF\Psi = S(u, T)\delta(z - z_0), \tag{2}$$

where L is the translation operator which takes into account elastic and inelastic scattering processes, $F = e\left[u\frac{\partial}{\partial T} + \frac{1}{pv}\frac{\partial}{\partial u}(1 - u^2)\right]$ is velocity,

p is the pulse, T is the kinetic electron energy, u = cos θ, θ is the angle between the electron pulse vector and axis Oz and S is a function of the fast electron source.

To close the system of equations (1) and (2), one must know the law which describes the dependence of conductivity on the radiation field:

$$\sigma = \sigma[\Psi], \tag{3}$$

which takes into account the variation of the state of the medium due to the effect of the SEP. Since this law is not known in the general case, we shall assume that the conductivity of the medium is determined experimentally.

The following modification of higher-order perturbation theory was used to solve the system of equations (1) and (2) with known conductivity $\sigma(z)$. Let the perturbation operator have the form

$$\hat{V} = E\hat{F}, \tag{4}$$

Then, having represented $\Psi = \sum_{j=0}^{\infty} \psi^{(j)}$ and $E = \sum_{j=0}^{\infty} E_j$ so that Ej is found from equation (1) by $N^{(j)}$, which is in turn calculated by $\psi^{(j)}$, we find the following formulas for calculating the terms of the series $\psi^{(j)}$ from equations of perturbation theory:

$$\psi^{(j)} = \hat{G}Q^{(j)}(\psi^{(0)}, \psi^{(1)}, \ldots \psi^{(j-1)}), \tag{5}$$

where

$$Q^{(j)} = F[(E_{vn} + \sum_{i=0}^{j} E_i)\psi^{(j-1)} + E_{j-1}\sum_{i=0}^{j-2}\psi^{(i)}]; \tag{6}$$

$\hat{G}$ is a nonperturbed Green operator and E_{vn} is the electric field created by the potential difference applied to the matter.

The explicit form of $E_{vn}(z)$ and $E_j(z)$ can be found from solution of equation (1) with boundary conditions for potentials $\varphi(z_0) = \varphi_0$ and $\varphi(z_1) = \varphi_1$:

$$E_{vn}(z) = -(\varphi_1 - \varphi_0)/\sigma(z)\Sigma(z); \tag{7}$$

$$N_J(z) = -\frac{j_A}{\sigma(z)}\left[f_J(z) - \frac{1}{\Sigma(z_1)}\int_{z_0}^{z} dz' f_J(z')/\sigma(z')\right], \tag{8}$$

where

$$\Sigma(z) = \int_{z_0}^{z} dz'/\sigma(z'); \; f_J(z) = \int_{z_0}^{z} dz' N^{(J)}(z')/j_0; \; j_A = ej_0; \; j_0$$

is the particle current density.

It follows from formula (5) that the problem of SEP passage through the matter reduced to solution of J (J is the number of terms of the series of perturbations) of nonperturbed transfer problems. The nonperturbed problem of electron transfer through the matter was solved by the multistep method in the continuous trajectory model which is described in [4].

Higher-order order perturbation theory was successfully applied in [5] to solution of the fast electron transfer problem in a dielectric with external electric field. The characteristics of realizing the method of perturbations were also described and the problem of convergence of the solution is also investigated in the same source.

Results of calculations and discussion. The most important in the problem of SEP interaction with matter is that of energy losses by the electron beam during electron passage through the matter. This problem occurs when solving problems on creation and heating of a plasma with high density by an electron beam in experiments on thermonuclear fusion, during development of detectors for SEP, during use of SEP for purposes of radiation technology and so on. Therefore, this paper is devoted mainly to calculation and analysis of the distributions of fast electron energy losses within matter as a function of the thickness of the layer of matter and the atomic number of the element. The lost energy distribution in inelastic fast electron collisions with atoms of the medium with regard to a single impinging electron was calculated by the formula

$$D(z) = \frac{1}{j_0}\int_{2\pi} d\Omega \int_{T_n}^{T_m} dT B(T)\Psi(z, u, T), \tag{9}$$

where B(T) is the specific fast electron energy losses having energy T, T_m is the upper bound of the fast electron spectrum and T_n is the threshold energy below which the electrons were regarded as thermalized. The value of T_n was usually taken as equal to several percent of the initial electron energy in the calculations.

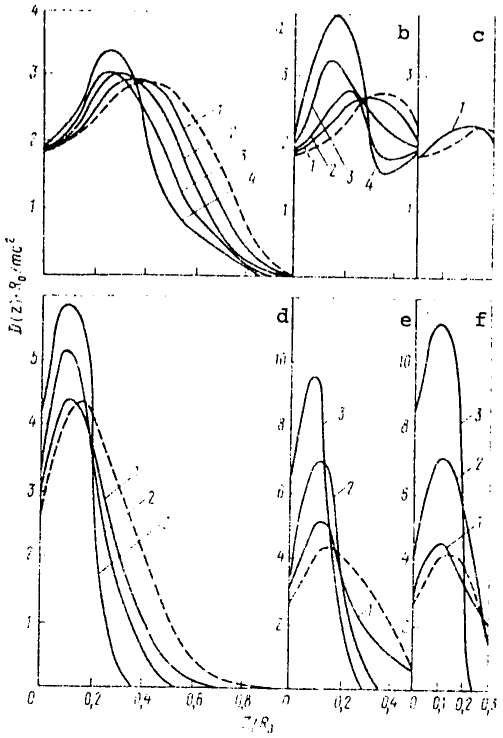

Figure 1. Distribution of Energy Lost in Inelastic Collisions by Electrons with Initial Energy of 1 MeV in Carbon (a, b and c) and copper (d, e and f) with different thickness of the matter Δz as a Function of E_A/ρ_m [(MV·cm^2)/g] (- - - - - $E_A = 0$): a = $\Delta z/R_0 = 1$; E_A/ρ_m = 1.0 (1); 2.0 (2); 2.5 (3) and 3.0 (4); b-- $\Delta z/R = 0.5$; E_A/ρ_m = = 10.0 (1); 20.0 (2); 22.5 (3) and 25 (4); c-- $\Delta z/R_0$ = = 0.3; E_A/ρ_m = 250.0 (1); d-- $\Delta z/R = 1$; E_A/ρ_m = = 3.0 (1); 5.0 (2) and 7.0 (3); e-- $\Delta z/R_0 = 0.5$; E_A/ρ_m = 10.0 (1); 13.0 (2) and 15.0 (3); f-- $\Delta z/R$ = = 0.3; E_A/ρ_m = 30.0 (1); 40.0 (2) and 50.0 (3)

$$T_0 = W_l + W_n + W_{corp}, \tag{10}$$

where $W_l = \int_{z_0}^{z} I(z)\,dz$ is the total energy loss of the particle

in inelastic collisions, W_k is the energy loss of the particle to coulomb interaction and W_{otr} is the energy carried away from the medium by the reflected particles and radiation.

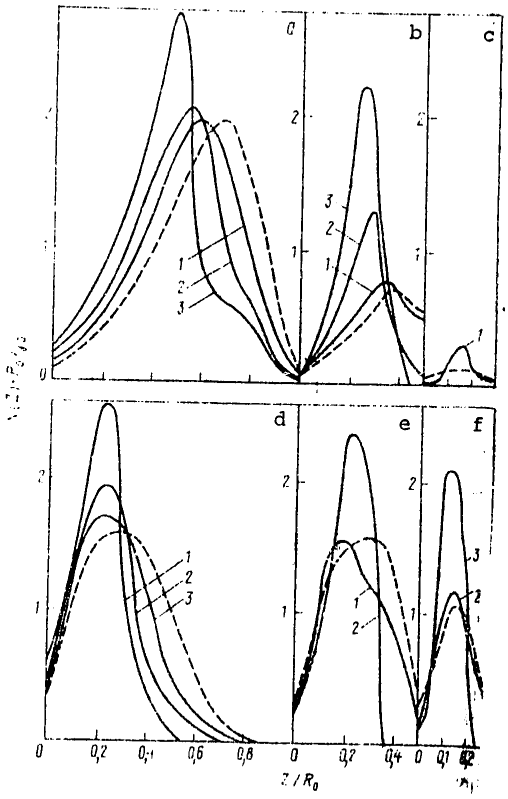

Figure 2. Thermalized Electron Distribution at Half-Depth of Matter (the notations are the same as in Figure 1)

In the steady-state case, the electric field energy created by thermalized electrons is used to create current $j_\sigma = \sigma E$. The work of charge displacement, according to Joule-Lentz law, is used to heat the matter. Calculated for a single impinging electron, this work is determined by the formula

$$W_{\text{ц}} = \frac{1}{j_0}\int_{z_0}^{z_1} dz\sigma E^2(z) = \int_{z_0}^{z_1} dz\,\frac{eE^2(z)}{E_A}. \qquad (11)$$

Calculations showed that 20 percent initial energy is achieved at $\Delta z/R_0 = 1\ W_k$ for $E_A/\rho_m = 3$ (MV·cm^2)/2 in matter with Z = 6 and will obviously increase with an increase of E_A/ρ_m.

Thus, analyzing the process of SEP interaction with matter, one can conclude the existence of two mechanisms of heating the matter by a charged particle beam: transfer of energy to the matter due to inelastic fast electron scattering processes on the atoms of the matter and conversion of the energy of fast electron interaction with the electric field to thermal energy with resorption of the space charge creating this field.

Based on the results presented in Figures 1, a and d and 2, a and d, we reach conclusions with respect to the role of the scattering properties of the medium in formation of distributions D and N. Since the elastic electron scattering cross-section is approximately Z^2 (Z is the atomic number), a considerable part of the electrons passes through the minimum potential during their propagation through matter with low atomic number and enters the region of an accelerating field. Therefore, all the distributions for matter with Z = 6 have "tails," formed by these electrons. The large elastic scattering cross-section in heavy matter makes the potential hole "impassable" for almost all particles.

A situation similar to that considered is also observed for thinner targets (see Figure 1, b and c and Figure 2, b and c). As follows from these figures, higher values of E_A are required for significant deformation of distributions than for a semi-infinite medium. This is explained by the fact that only part of the electrons is thermalized in a barrier of finite thickness and the fraction of particles thermalized in the barrier is determined mainly by the scattering properties of the medium.

Thus, approximately three percent of all particles are thermalized in a layer of matter with Z = 6 having thickness of 0.3 R_0 and more than 20 percent are thermalized in the same layer at Z = 29. This means that considerably greater densities of the impinging beam are required in a layer of matter with small value of Z than in one with large value of Z for complete stopping of the beam. It is obvious from Figure 1, c and Figure 2, c that even at $E_A/\rho_m = 250$ (MV·cm^2)/g, the distribution deformation is insignificant while the maximum depth of the potential hole comprised approximately 0.2 MeV (see Figure 3, c). Formation of a potential hole for heavy matter leads to stopping of the beam in the layer and all the beam energy is released in the volume of the layer. It is obvious from Figure 1, f that energy exceeding almost twofold that which is released during passage of a low-intensity beam is released in the target. This effect may apparently be increased significantly by selecting thinner layers of heavier elements.

Thus, the investigations permit one to explain the phenomena of abnormal energy absorption in thin oils, observed in the experiments [1], and to reduce the depth of electron penetration into the matter [2]. The reason

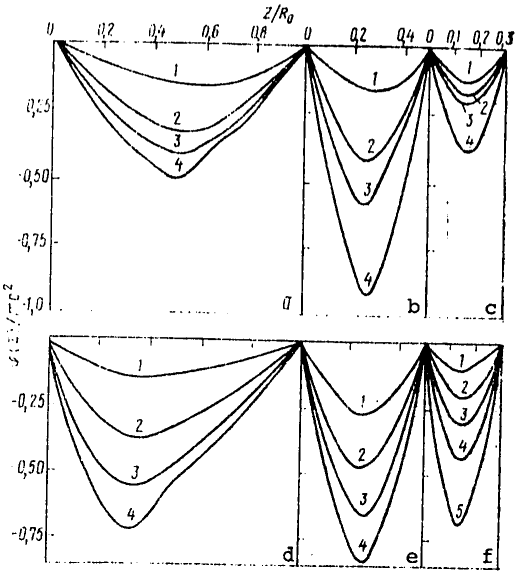

Figure 3. Potential Distribution Through Depth of Matter (the notations in a, b, d and e are the same as in Figure 1): c-- $\Delta z/R_0 = 0.3$; E_A/ρ_m = 100.0 (1); 150.0 (2); 200.0 (3) and 250.0 (4); f-- $\Delta z/R_0 = 0.3$; E_A/ρ_m = = 10.0 (1); 20.0 (2); 30.0 (3); 40.0 (4) and 50.0 (5)

for the occurrence of these effects is the effect of the coulomb field whose source is the space charge created by thermalized electrons due to the poor conductivity of the plasma formed due to the effect of the SEP during explosion of the target on fast electron transfer. The plane configuration considered here does not permit one to take into account the effect of the magnetic field of the SEP on passage of electrons in matter. However, the insignificance of the effect of the magnetic field within the target matter was pointed out in [8], which can indirectly be regarded as confirmation of the correctness of the approach formulated above.

The authors express thanks to O. B. Yevdokimov, A. M. Kol'chuzhkin and A. V. Lappe for useful discussions.

BIBLIOGRAPHY

1. Bogolyubskiy, S. P. et al, PIS'MA V ZHETF, Vol 24, No 4, 1976.

2. Nakai, S., K. Imasaki and C. Yamanaka, NUCLEAR FUSION, Vol 17, Supplement, 1977.

3. Vorob'yev, A. A. and O. B. Yevdokimov, IZV. VUZOV SSSR, FIZIKA, No 2, 1972.

4. Vorob'yev, A. A. and A. P. Yalovets, ATOMNAYA ENERGIYA, Vol 36 No 3, 1974.

5. Shevelev, G. B. and A. P. Yalovets, IZV. VUZOV SSSR, FIZIKA, No 10, 1978.

6. Rudakov, L. I., FIZIKA PLAZMY, Vol 4, No 1, 1978.

7. Bogdankevich, L. S. and A. A. Rukhadze, USPEKHI FIZ. NAUK, Vol 103, 1971.

8. Yonas, G., Electron Beam Fusion Progress Report, Sand. 76-0410, 1976.
[8144/0538-6521]

6521
CSO: 8144/538

NUCLEAR PHYSICS

UDC 539.1

LENINGRAD INSTITUTE OF NUCLEAR PHYSICS IMENI B.P. KONSTANTINOV TRENDS AND DEVELOPMENT PROSPECTS DISCUSSED

Moscow VESTNIK AKADEMII NAUK SSSR in Russian No 7, 1979 pp 3-11

[Article: "Regarding the Operations and Development Prospects of the USSR Academy of Sciences Leningrad Institute of Nuclear Physics imeni B.P. Konstantinov"]

[Text] The USSR Academy of Sciences Leningrad Institute of Nuclear Physics (LIYaF) imeni B.P. Konstantinov was created in 1971 on the basis of a branch of the FTI [Physicotechnical Institute] imeni A.F. Ioffe in Gatchina.

Now working at the institute are more than 2000 people. Included in the institute's structure are four large laboratories: high-energy physics, neutron research, molecular and radiation biophysics, and theoretical physics--as well as a number of institutewide scientific and technical divisions.

In operation at the institute are very large units, such as a beam-type research reactor of the VVRM [water-moderated, water-cooled magnetic reactor] type with a thermal capacity of 16 MW and a maximum neutron flux of $3 \cdot 10^{14}$ $1/cm^2 \cdot s$, an accelerator--a proton synchrocyclotron with a power of 1 GeV and a current in the extracted beam of up to 1 μA, an electron synchrotron with a maximum energy of 100 meV, and a neutron generator. In existence here is an advanced computer system which in addition to the ordinary computing functions performs the functions of controlling, gathering and processing data.

The Presidium of the USSR Academy of Sciences has discussed the key trends and development prospects of the Leningrad Institute of Nuclear Physics. A report was given by the director of the institute, USSR Academy of Sciences Corresponding Member O.I. Sumbayev.

O.I. Sumbayev's Report

The key scientific trends undergoing development at LIYaF are the physics of elementary particles and of their interactions, nuclear physics, solid

state physics, and molecular and radiation biophysics. In addition, under way at the institute are applied research and development on detectors of nuclear radiation, as well as in the area of radio electronics, physics, and the engineering of research reactors and accelerators.

The most well-known series of studies at LIYaF, performed under the guidance of USSR Academy of Sciences Corresponding Member V.M. Lobashev and awarded (together with Yu.V. Abov's group at the Institute of Theoretical and Experimental Physics) the Lenin Prize in 1974, has been devoted to an investigation of the nonconservation of space parity in nuclear forces. As the result of research based on the new so-called integrated procedure for experimentation, there has been definitely proven a fundamentally important faint interaction between nucleons in a nucleus, confirming the theory of the universality of faint interactions. The results of studies by V.M. Lobashev's group in subsequent years have received both qualitative and quantitative confirmation in other laboratories (table).

Table. Effect of Nonconservation of Space Parity in Nuclear Forces

1) Ядро	2) Экспериментальный эффект	3) Авторы	4) Год	5) Среднее значение с учетом последующих работ
$n+p \to d+\gamma$	$P_\gamma = -(1{,}30 \pm 0{,}45) \cdot 10^{-6}$	Лобашев и др. 6)	1972	–
^{41}K	$P_\gamma = +(1{,}9 \pm 0{,}3) \cdot 10^{-5}$	Лобашев и др.	1969	–
^{75}As	$P_\gamma = -(6{,}0 \pm 2{,}0) \cdot 10^{-5}$	Vanderleeden a. o.	1972	–
^{114}Cd	$P_\gamma = -(6{,}0 \pm 1{,}5) \cdot 10^{-6}$	Alberi a. o.	1972	–
^{175}Lu	$P_\gamma = +(4{,}5 \pm 1{,}0) \cdot 10^{-5}$	Лобашев и др.	1967	$+(5{,}5 \pm 0{,}5) \cdot 10^{-5}$
^{180}Hf	$P_\gamma = -(2{,}8 \pm 0{,}45) \cdot 10^{-3}$	Jenscke and Bock	1970	–
^{181}Ta	$P_\gamma = -(6{,}0 \pm 1{,}0) \cdot 10^{-6}$	Лобашев и др.	1967	$-(5{,}2 \pm 0{,}5) \cdot 10^{-6}$
^{111}Cd	$A_\gamma = -(3{,}7 \pm 0{,}9) \cdot 10^{-4}$	Абов и др. 7)	1965	–
^{117}Sn	$A_\gamma = +(8{,}1 \pm 1{,}3) \cdot 10^{-4}$	Данилян и др. 8)	1976	–

Key:
1. Nucleus
2. Experimental Effect
3. Authors
4. Year
5. Mean value taking into account subsequent studies
6. Lobashev et al.
7. Abov et al.
8. Danilyan et al.

Another important study by this same group involves measuring the electric dipole moment of a neutron. In recent years in the largest laboratories in the world attempts have been made to detect this moment, since its existence is possible only with the nonconservation of so-called combined, or time, parity. The unified theory of faint and electromagnetic interaction of Vaynberg-Salam, which is quite popular today, postulates the existence of a neutron dipole moment in the range of $(1 \text{ to } 10) \cdot 10^{-25}$ e·cm.

The most accurate experimental upper limit of the moment, arrived at in 1977 in the best research reactor in the world at the Laue-Langevin Institute in Grenoble equals $< 30 \cdot 10^{-25}$ in the same units with a degree of certainty of 90 percent. Thus, the severalfold improvement in accuracy in these experiments has been of fundamental importance.

At LIYaF for the first time has been implemented a method employing so-called ultracold neutrons, which has made possible in research on the dipole moment of neutrons a considerably lower level of systematic errors and has opened the way to a further improvement in accuracy. (The limit reached as of today equals $< 15 \cdot 10^{-25}$.)

In the high-energy physics laboratory has been suggested and implemented a new precise method of measuring the small-angle scattering cross sections of elementary particles by means of a special ionization chamber. The universality of this method has made it possible to carry the experiment over to the pion beams of the Serpukhov accelerator, the largest in the USSR, and then to the beams of the largest proton accelerator in Europe at CERN [European Council for Nuclear Research].

The question of variations in the full scattering cross sections of particles of extremely high energy is one of the most important in high-energy physics. The preliminary results of research conducted at the institute indicate that the total cross sections in the energy region of up to a few thousand GeV/s evidently increase at the maximum permissible rate. In 1979 an experiment will be continued at CERN in the region of approximately doubled energies.

In the high-energy physics laboratory, employing a unit with high resolution, a series of studies has been conducted for the purpose of studying the distribution of neutrons in the nucleus and, consequently, nuclear matter. Systematic measurements have been made on a score of nuclei from helium to lead. Apparently in these studies has been gained the most reliable information on the distribution of matter in nuclei.

Then the writer of the report dwelled on a scientific trend specific to LIYaF--precision crystal diffraction x-ray and gamma spectroscopy.

As early as by the beginning of the 60's ways had been found of improving the transmission and precision of instruments of certain types for this area of research. Later a new procedure made it possible to discover interesting effects, such as the so-called chemical (caused by the structure and filling in of valence shells of an atom) shift in fundamental x-ray lines in relatively heavy elements; the isotropic (caused by the distribution of the electric charge in nuclei) shift; and the broadening of x-ray lines, associated with so-called hyperfine interaction--interaction between nuclear spin and a K electron. The first two effects have become the basis for new experimental methods of investigating structure--studying crystal chemical bonds and charge distributions in nuclei. These methods have won

recognition in a number of leading laboratories of the world. Recently at CERN and LIYaF were discovered two new varieties of the x-ray effects caused by hyperfine interaction: high (up to 1 eV) energy shifts of x-ray K lines, excited in the disintegration of radioactive nuclei after K capture and internal conversion, respectively. Both new effects are interesting in terms of possibilities for applying them for the purpose of measuring the magnetic moments of excited states of nuclei.

Then the speaker spoke of the application of a diffraction spectrometer developed at LIYaF for the purpose of investigating x-radiation from the capture of pions by nuclei. The distinctive feature of this method consists in the fact that the target in which mesons are generated is combined with the source in which they are captured, emitting x-radiation. The value of the mass of a pion precisely defined by this method has made it possible to refine (reduce) the value of the limit of the mass of a u-meson neutrino.

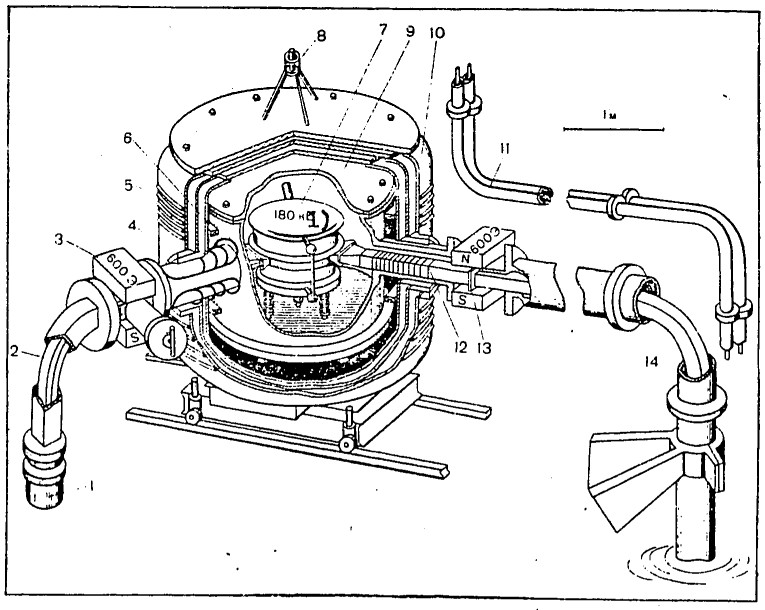

Figure 1. Unit for Measuring Electric Dipole Moment of a Neutron, Utilizing Ultracold Neutrons: 1--dual chamber detector; 2--double neutron guide; 3--polarization analyzer; 4--coils creating magnetic field gradient; 5--demagnetizing coils; 6--coils creating permanent magnetic field in

[Figure and caption continuation and key on following page]

chambers for storing neutrons; 7--chambers for storing neutrons; 8--ferroprobe sensor of system for stabilizing external magnetic field; 9--vacuum chamber; 10--magnetic shields; 11--cryopipelines; 12--input solenoid for variable magnetic field; 13--polarizer; 14--neutron guide; 15--lead shield; 16--fuel elements of reactor

Key:
1. 180 kV

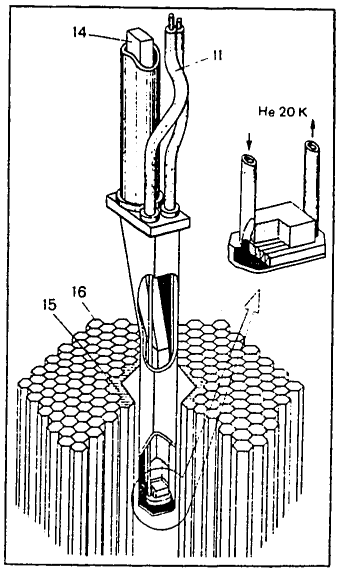

Figure 1. [Continued]

The possibility has also arisen of determining precisely defined values of the amplitude of strong interaction between a pion and nucleons of a nucleus, which are important for solving the question of the existence in nuclei of Migdal's pion condensate.

The precise method makes it possible to investigate also short-living particles. Estimates have demonstrated that it is already totally realistic to register x-ray lines from Σ, Ξ or even Ω hyperons, by precisely defining not only values of masses, but also of magnetic moments and spins themselves. It is planned to carry out this research in Serpukhov.

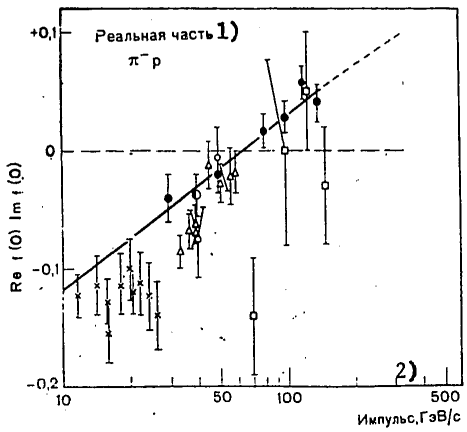

Figure 2. Data on the Dependence of the Forward πp-Scattering Cross Section on the Momentum of Mesons, Obtained in LIYaF Experiments Conducted at CERN: black dots--LIYaF-CERN (1978); semishaded dots--LIYaF-IFVE [Institute of High-Energy Physics]-OIYaI [Joint Institute of Nuclear Research] (1978); squares--Batavia (1975); diamonds and white dots--IFVE (1976); X's--Brookhaven (1967); dotted line--Holger, dispersion relations (1977)

Key:
1. Real half
2. Momentum, GeV/s

A great portion of the work on solid state physics is concentrated in an individual section of the neutron research laboratory, intimately allied with a section of the theoretical physics laboratory. Research is being conducted basically by means of polarized neutrons, i.e., magnetic phenomena are being studied primarily. In recent years considerable attention has been devoted to studying so-called critical phenomena near points of magnetic phase transitions of the second kind--in connection with verification of the conclusions of the well-known scaling theory, or the similitude hypothesis. Conducive to the success of this trend has been a new procedure--the so-called vector analysis of polarizations, whose idea consists in the fact that if for an individual neutron it is possible to measure simultaneously only one spin projection, then for a neutron beam

it is possible to measure all three projections, i.e., to determine the polarization vector of the beam before and after scattering. The practical implementation of this method has considerably expanded the informativeness of experiments on scattering, having made it possible to solve a number of qualitatively new problems.

Among work done at the molecular and radiation biophysics laboratory, the speaker singled out the following trends. In the investigation of radical reactions--such as primary reactions arising under the effect of radiation on biological systems, both of free radicals and of radicals activated under the effect of enzymes of states--a method has been suggested for the detection of electron paramagnetic resonance from rotation of the plane of polarization of SHF oscillations. This method has made it possible to increase sensitivity by two orders of magnitude. Later on its basis was developed a modulusless method of recording EPR signals making it possible with a very high degree of accuracy (of up to 10^{-3}) to record the form of absorption and dispersion lines without a loss of sensitivity.

It has become possible to study enzymatic reactions directly in an aqueous solution, in spite of high dielectric losses. As a result it has been possible for the first time to demonstrate the formation of free radicals as intermediate stages of two oxidative enzymatic reactions catalyzed by oxidases.

This work has opened up a new trend in the study of biochemical processes.

A second fundamentally important study by the molecular and radiation biophysics laboratory concerns protein biosynthesis. It is known that protein biosynthesis takes place in a special particle--a ribosome--which has two working positions. In one of them is sorbed the incomplete protein chain, and in the other the next amino acid, i.e., the next link in the chain. Both reacting molecules form chemical compounds with the transport RNA--a low polymer bearing amino acids and making possible their proper selection. The most interesting stage of synthesis is translocation, i.e., the transition of the transport RNA with a growing chain from one position to another after completion of the next addition step.

As the result of investigations of the thermodynamics of the binding of transport RNA in both positions in the ribosome, it was revealed that transport RNA exists in the form of two isomers of quite different configurations. Just the changing of one isomer into another, because of the loss of a magnesium ion, so alters the molecule that it tends to cross from the first position over into the second. This study has evoked great interest in the USSR and abroad.

Of great practical importance has been the laboratory's work on the purification of viruses by the chromatography method for the purpose of producing influenza and tick-borne encephalitis vaccines. This new original technology has been patented in all developed industrialized countries and is now being introduced in our country on a large scale.

Another task of the molecular and radiation biophysics laboratory which is of an applied nature relates to environmental protection and the monitoring of production hazards. It is known that much waste of the chemical industry contains carcinogenic substances. It is necessary to equip sanitary and epidemiologic stations with express methods of analyzing for potential carcinogens.

In the laboratory has been proposed a method for testing for mutagenesis special strains of yeasts. These organisms contain cytochrome P450 and therefore are able to activate carcinogenic products similarly to how this takes place in the human body. In addition, an individual yeast strain quickly mutates and thereby changes color, which makes it possible to create a simple method of testing potentially toxic products. This method is now passing tests within the framework of an international agreement.

The theoretical physics laboratory participates in many experimental studies by LIYaF. The ideological influence of theoreticians has been certain, on the development of research on small-angle scattering, in formulation of the experiment relating to the revelation of the asymptotic behavior of full cross sections. Associates of the laboratory have taken part in calculations of Glauber scattering of protons in nuclei and have made calculations in the investigation of chemical shifts of x-ray lines. The experimental and theoretical solid state physics sections work in close contact. But, of course, the theoretical physics laboratory is primarily occupied with its own problems. The most important results arrived at by the institute's theoreticians have been the creation of a phenomenological theory of processes of the interaction of non-leptons at superhigh energies; investigation of the intensely inelastic processes of the interaction of leptons with non-leptons within the framework of the quantum field theory; the development of a new method of investigating high orders of the perturbation theory of the quantum field theory; and the discovery of fundamental ambiguities in quantization of non-Abelian calibration theories outside the framework of the perturbation theory.

Of decisive importance for the overwhelming majority of investigations carried out at the institute, the speaker emphasized, are the parameters of the key units at LIYaF.

The accelerator--a 1 GeV proton synchrocyclotron--the largest accelerator of its class in the world--has become obsolete in connection with the appearance of accelerators of a new generation with stable focusing. The job was undertaken of studying the latent capabilities of the unit and after some modernization its parameters were considerably improved.

Below are given the key parameters of the secondary beams which the accelerator today has at its disposal.

Parameters of meson beams: π^- mesons (W = 300 to 600 MeV)--10^6 particles/s; π^+ mesons (W = 300 to 600 MeV)--$3 \cdot 10^6$ particles/s; μ^- mesons (P = 120 MeV/s)--$6 \cdot 10^4$ particles/s; μ^+ mesons (P = 120 MeV/s)--$2 \cdot 10^5$ particles/s.

Parameters of neutron beams: n (W = 400 to 900 MeV)--10^6 particles/s; $n_{imp\ [pulse]}$ (W = 1 eV to 1 MeV)--10^4 particles/$cm^2 \cdot s$, length of pulse--7 to 30 ns ("Gneiss").

Polarized protons: P (W = 990 MeV, 33 percent)--10^7 particles/s.

Medical channel: P (W = 1 GeV, D = 3 to 5 mm)--10^9 particles/s (15 to 18 Trad in approximately 15 min).

The VVRM reactor has been used at LIYaF since 1959. As the result of subsequent modernization its capacity has grown from 10 to 16 MW, the number of horizontal channels has been increased and an above-reactor hot cave has been created, which has enabled the unique opportunity of carrying out complicated experiments directly in the active zone. Able to serve as an example is the experiment on determining the dipole moment of a neutron, about which was spoken above. Now a project has been developed for thorough modernization of the reactor with a simultaneous increase in its capacity to 30 MW. The implementation of this project will make it possible to extend the unit's life another 20 years.

The future of nuclear physics research involves completion of the construction of the new modern PIK research beam reactor with a laboratory complex. The reactor will have a thermal capacity of 100 MW and a maximum thermal neutron flux of $4 \cdot 10^{15}$ neutrons/$cm^2 \cdot s$. The reactor must be equipped with sources of cold and hot neutrons, as well as an advanced system of neutron guides which deliver hot and cold neutrons to a separate room where provision has been made for the additional location of about 20 experimental units under low-noise conditions. In the main experimentation room provision has been made for reducing the vibration level, which is necessary for the formulation of precise experiments.

Conditions have been provided for utilization of the reactor by other institutes; therefore the startup of the PIK complex can enable a qualitatively new level of individual research over the entire country.

Being an academic institute, LIYaF regards its main objective as the development of fundamental research. But much attention is devoted also to work of an applied nature. The applied work done by the biological laboratory has already been mentioned. Of work along the medical and biological line the speaker named also the successful utilization of a proton beam specially formed at LIYaF in the clinic, added onto the accelerator building, of the USSR Ministry of Health Leningrad Roentgen Radiology Institute--for cancer therapy, and the production at the institute of a number of pharmacological preparations tagged with iodine. Part of the applied research involves the development of radiation detectors and the automation of measurements and data processing, in particular, the creation of an original system with a holographic memory, designed for recording and retrieving patent information. In addition to the projects for the PIK and VVRM reactors, with the participation of LIYaF projects have been developed for modernizing

reactors of the same type in a number of CEMA member countries, and work is successfully under way on creating improved fuel elements for research reactors of several types.

Figure 3. Model of PIK Complex: 1--reactor and main experimentation room; 2 and 3--technological buildings; 4--administration building and sanitary and decontamination centers; 5--physics building (computer and laboratory areas for physicists); 6--neutron guide building (in basement, technological laboratories for attending to experiments); 7--cryogenic building (equipment of cold neutron source and detritization unit); 8--ventilation center. The buildings are connected by a heated circular tunnel for walking.

There are reasons to believe, said the speaker in his conclusion, that in the seven years which have passed since its formation LIYaF has become one of the leading institutes of the USSR Academy of Sciences.

Discussion of Report

Academician M.A. Markov discussed in detail the achievements of the recently created Leningrad Institute of Nuclear Physics imeni B.P. Konstantinov, which in a brief time has won international scientific authority. An analysis of the institute's operations has demonstrated that in all the trends being developed by it new procedures have been developed and employed, which have made it possible to achieve effective results even with units inferior in their parameters to the best foreign ones. For example, in measuring the dipole moment of a neutron, because of a clever procedure with LIYaF's reactor was achieved a result more accurate than with the most perfect reactor in the world in Grenoble. The new so-called integrated procedure has been used also in investigations of faint interactions.

In the institute was suggested and implemented a new method for measuring the small-angle scattering cross sections of elementary particles, which has made it possible to arrive at results greatly superior in accuracy to similar data from employing different foreign units. The same applies to studies in the field of solid state physics and biology.

M.A. Markov noted that the institute's future depends to a great deal on implementation of the project for the high-capacity PIK reactor and stressed the need to render assistance to the institute in highly rapid construction of the reactor and in modernizing the accelerator in existence there.

USSR Academy of Sciences Corresponding Member B.S. Dzhelepov proposed a number of organizational measures for the purpose of coordinating the scientific institutions of Leningrad working on nuclear physics.

USSR Academy of Sciences President Academician A.P. Aleksandrov spoke in conclusion. He noted the outstanding achievements of LIYaF in the field of nuclear physics and solid state physics. In some of the fundamental research conducted by the institute the best results in the world were achieved. A.P. Aleksandrov suggested to the USSR Academy of Sciences Presidium that special consideration be given to the question of further development of the institute and that a decision be made regarding the capital investment required for the purpose of creating the PIK reactor.

Decree

The Presidium of the USSR Academy of Sciences has approved the operations of the USSR Academy of Sciences Leningrad Institute of Nuclear Physics imeni B.P. Konstantinov relating to the development of fundamental research in the field of nuclear physics and the physics of elementary particles, theoretical physics, solid state physics and molecular and

radiation biophysics, as well as to the solution of national economic problems. Note has been made of the initiative and important achievements of the USSR Academy of Sciences LIYaF in the development and erection of the unique PIK high-flux research nuclear reactor, as well as in the modernization of the 1 GeV synchrocyclotron.

USSR Academy of Sciences Vice President for Capital Construction V.P. Isayev and the management of the USSR Academy of Sciences LIYaF have been entrusted with taking the necessary measures for the very rapid entry of the PIK reactor into effective service (making sure, in particular, of the start of the construction of laboratory buildings by not later than 1981), as well with beginning in the 11th Five-Year Plan period work relating to mastery of the synchrocyclotron's high intensity.

The Presidium of the USSR Academy of Sciences has found advisable the further development at the USSR Academy of Sciences LIYaF of work relating to the automation of measurements, and in particular the speeding up of the creation of the experimental production of electronic equipment up to the KAMAK [expansion unknown] standard.

CSO: 1862
8831

OPTICS AND SPECTROSCOPY

UDC 535.6:681.7.013.84

THE COLOR AND VISUAL CONTRAST OF AN IMAGE ON THERMOCHROMIC MATERIAL FTIROS

Leningrad ZHURNAL TEKHNICHESKOY FIZIKI in Russian Vol 49 No 5, 1979
manuscript received 6 Oct 78 pp 1008-1012

[Article by B. P. Zakharchenya, Ye. I. Terukov, F. A. Chudnovskiy and Z. I. Shteyngol'ts, Physicotechnical Institute imeni A. F. Ioffe of the USSR Academy of Sciences, Leningrad]

[Text] The results of investigating the optical characteristics of thermochromic material FTIROS based on vanadium oxides are presented. Data on the visual contrast of an image are given as a function of the optical thickness of the vanadium oxide layer and of the material of the reflecting sublayer and the angular dependence of the brightness coefficient is also investigated.

The new thermochromic material FTIROS based on vanadium oxides, suitable for recording, storage and display of optical information, was proposed in [1]. The basis of operation of the material is the phenomeno of metal-dielectric phase transition of first kind observed in vanadium oxides [2]. FTIROS material is a parametric interference wideband light filter which reflects light. The initial color of FTIROS when it is illuminated by white light is determined by the spectral dependence of the reflection coefficient in the visible region of the spectrum, which is mainly determined by the optical thickness of the vanadium oxide layer and by the design formulation of the material.

When FTIROS is heated to approximately 65°C, the metal-dielectric phase transition, accompanied by sharp variation of the complex refractive index, occurs in the right-modulating vanadium oxide layer. This causes redistribution of the function of the spectral reflection coefficient in the visible region of the spectrum and leads to variation of the initial color of the material.

The use of FTIROS for passive display panels [3], color indicator boards, displays and so on raises the question of the color characteristics and visual contrast of an image on this material.

An objective method for calculating the color contrast of an image on FTIROS was proposed (by analogy with the brightness contrast for black-white images) in [4]. It was shown in the paper that the color and visual contrast of an image on the given material varies over a wide range as a function of the thickness of the vanadium oxide layer and this circumstance should be taken into account in its practical application.

The dependence of the color characteristics and visual contrast of an image on thermochromic material FTIROS on the thickness of the vanadium oxide layer was investigated in this paper and these parameters were optimized for visual readout of information.

1. The Experimental Installation and Method of Measurements

The method of calculating contrast, proposed in [4], despite objectivity, is related to a large volume of calculations. We used the following method of measurements to simplify determination of visual contrast and also to investigate the angular dependence of the brightness coefficient of FTIROS material.

A diagram of the experimental installation is shown in Figure 1. FTIROS was placed on a heater, which, when switched on, caused the metal-dielectric phase transition which leads to variation of the color of the material. The specimen was illuminated at an angle of approximately 90° to the surface of the material of the lighting lamp with known color temperature and the current through the lamp was monitored constantly during measurements. The lighting radiation was passed through a condensing lens, milk glass and correcting light filters, which produced uniform illumination in the plane of the specimen with spectral composition close to a source of type C (T = 6,500K), which simulates natural lighting. The microscope was focused on the thermochromic material and in this case a section of FTIROS 7 mm in diameter fell into the visual field. The use of a microscope-autocollimator permitted an estimate of the initial angular position of the specimen surface with respect to the axis of the installation. The light reflected by the material entered the optical system of the microscope on a photomultiplier, in front of which light filters were installed, which guide the curve of spectral sensitivity of the FEU to the curve of visibility of the eye. The integral correction error of the spectral characteristic of the FEU in the visible region of the spectrum was approximately 1 percent. The output signal of the FEU was recorded by a digital voltmeter.

Thus, the installation was a photometer-brightness meter which measures the average light intensity reflected from the section of FTIROS at angle d/f, where d is the diameter of the microscope objective and f is its focal distance. The long focal distance of the microscope objective made it possible to incline it by angle $\theta = \pm 60°$ from the optical axis of the installation, while the table with the specimen had the capability of rotating around the axis of the installation. Because of this, it was

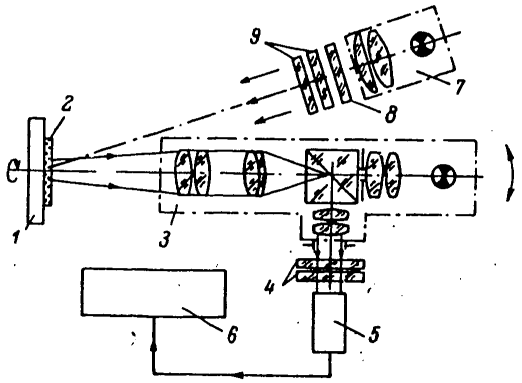

Figure 1. Installation for Investigation of the Contrast and Angular Dependence of Image Brightness Coefficient on FTIROS Material: 1--heater; 2--FTIROS specimen; 3--microscope-autocollimator; 4--correcting filters of FEU; 5--FEU-55; 6--VK2-20 digital voltmeter; 7--illuminator with condensing lens; 8--MS-13 milk glass; 9--filters which correct the lighting source

possible to take the angular dependence of the brightness coefficient of FTIROS material both on the direction θ and on the azimuth φ of observation. The brightness coefficient of the tested section of FTIROS was determined as $\beta = N/N_0$, where N is the reading of the voltmeter during reflection from the FTIROS and N_0 is the reading of the voltmeter during reflection from a plate coated with a layer of MgO with known reflection coefficient $\rho = 0.98$.

Visual contrast was determined by the expression $K_v = (N_1 - N_2)/N_1$, where N_1 is the voltmeter reading during reflection from the FTIROS to phase transition and N_2 is that after phase transition.

The angular dependence of the brightness coefficient was taken in the range of observation angles of $\pm$ 60° with spacing of 5° and the variation of the area of the monitored section, proportional to cos θ, was taken into account. The sensitivity of the installation was 5 percent of the value of the measured brightness.

2. Results of Measurements and Discussion of Them

Investigation of color characteristics. Specimens of FTIROS material were manufactured on polished and ground sitall substrates and were a thin-film structure produced during controlled oxidation of metallic vanadium. The

interference coloring of the specimens when they were illuminated by white light was determined by the optical thickness of the vanadium oxide layer and by the presence of a reflecting sublayer of metallic vanadium in the structure.

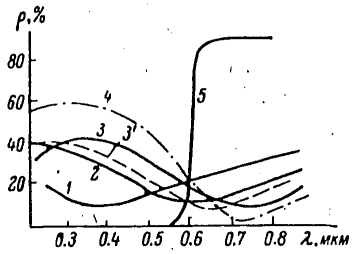

Figure 2. Spectral Functions of Reflection Coefficient of FTIROS Material: The optical thickness of the vanadium oxide layer nh (micron): 1--0.18; 2--0.3; 3--0.38 (path before phase transition); 3'--0.38 (path after phase transition; 4--dependence of reflection coefficient at nh = = 0.38 micron and with reflecting sublayer of aluminum; 5--dependence of light filter transmission coefficient in front of lighting source for contrast optimization

Typical spectral characteristics of FTIROS of different optical thickness are presented in Figure 2. The optical thickness was determined by the position of the interference minimum reflection without regard to absorption in the oxide layer by the formula $nh = \lambda/2$, where n is the refractive index, h is the geometric thickness of the oxide layer and λ is the wavelength corresponding to minimum reflection.

It is obvious from Figure 2 that the interference minimum can be found in any region of the visible spectrum as a function of the optical thickness of the vanadium oxide layer. This explains the variety of initial colors of FTIROS material. Variation of the color of the material during phase transition was caused by redistribution of the spectral function of the reflection coefficient in the visible region--by shifting of the interference minimum to the short-wave region of the spectrum (Figure 2, 3'). Variation of the colors of the material is presented in Figure 3, where the values of three-color coefficients of FTIROS before and after phase transition for specimens of different optical thickness are plotted on the color graph in the system XYZ. Three-color coefficients for lighting source of type C were calculated by the selected ordinate method described in [5].

It is obvious from Figure 3 that three-color coefficients of FTIROS before and after phase transition differ by a value considerably greater than the

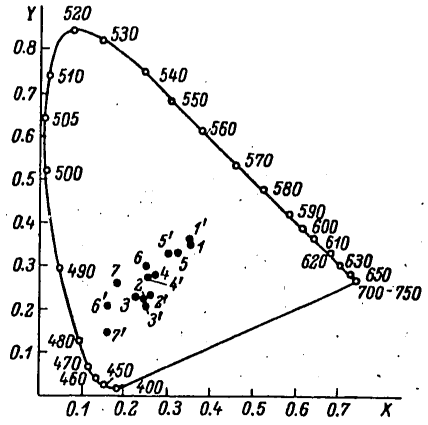

Figure 3. Position of Three-Color Coefficients of FTIROS Material on Color Graph as a Function of Optical Thickness of Vanadium Oxide Layer: nh, micron: 1 and 1'--0.19; 2 and 2'--0.3; 3 and 3'--0.32; 4 and 4'--0.38; 5 and 5'--0.4; 6 and 6'--0.31 (aluminum reflecting sublayer); 7 and 7'--0.38 (numbers with a prime are the value of three-color coefficients of the material after phase transition).

Color Transitions of FTIROS Material

(1) Оптическая толщина слоя окислов ванадия, мкм	Цвет материала (2)			
	до фазового перехода (3)		после фазового перехода (4)	
	наименование [*] (5)	обозначение [*] (6)	наименование [*]	обозначение [*]
0.19	Желтовато-зеленый (7)	V, 1:1	Светло-желтовато-зеленый (12)	VI, 1:4
0.3	Синевато-пурпурный (8)	12.0; 1:0.1	Пурпурный (13)	1.0—6/6
0.32	Синий (9)	13.0; 1:1	Синевато-пурпурный	14.0; чистый
0.38	Светло-синий (10)	13.0; 1:16	Темно-синий (14) (15)	12.0; 1:0.1
0.4	Серо-синий (11)	12.0; 1:32	Светло-синий (10)	13.0; 1:16

Key:
1. Optical thickness of vanadium oxide layer, micron
2. Color of material
3. Prior to phase transition
4. After phase transition

[Key continued on following page]

[Key continued from preceding page]

5. Name [7]
6. Notation [8]
7. Yellow-green
8. Blue-purple
9. Blue
10. Light blue
11. Gray-Blue
12. Light yellow-green
13. Purple
14. Bluish-purple
15. Dark Blue

light discrimination threshold of the eye for a given spectral region for specimens of material with optical thickness of the vanadium oxide layer greater than 0.2 micron [6], which permits one to distinguish the color of the material sufficiently clearly before and after phase transition. It should be noted that the appearance of a new color on a background of the initial color in our case is the result of subtraction of one complex color from another. This creates difficulties in determining the names of the colors of FTIROS material. Color transitions on FTIROS material are presented in the table as a function of the technology of manufacture. The names of the colors are taken mainly from [7] and, moreover, their notations are presented according to the newest colors standardized in the atlas [8].

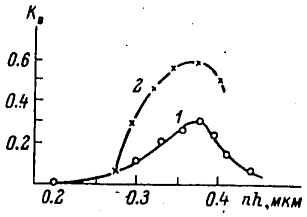

Figure 4. Dependence of Visual Contrast of Image on the Material on the Thickness of the Vanadium Oxide Layer: 1--reflecting sublayer of metallic vanadium; 2--reflecting sublayer of aluminum

The visual contrast of the image. The dependence of the visual contrast of the image on the optical thickness of the vanadium oxide layer for specimens of FTIROS material with reflecting sublayer of metallic vanadium is presented in Figure 4. The maximum contrast comprises approximately 0.3 with optical thickness of approximately 0.38 micron in this case. FTIROS specimens with reflecting sublayer of aluminum, which has a higher reflection coefficient in the visible region of the spectrum, were manufactured to increase the contrast. As one would expect, the interference minimum reflection of these specimens was expressed more sharply (Figure 2, 4), which permits one to obtain visual contrast of approximately 0.6 for optical thickness and also contrast equal to 0.38 micron (Figure 4, 2).

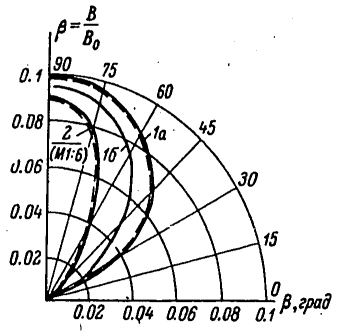

Figure 5. Indicatrices of Brightness Coefficient of FTIROS Material as a Function of Observation Angle: 1a--specimen with thickness of oxide layer of 0.38 micron on a ground substrate prior to phase transition; 1b--after phase transition; 2--specimen on reflecting substrate. The indicatrices of the brightness coeffficients for substrates without FTIROS are shown by the dashed line (the brightness scale is not followed in this case)

As can be seen from the table, the color transition light blue to dark blue is realized on FTIROS specimens with maximum contrast. Analysis of the dependence of the spectral reflection coefficient of FTIROS specimens with maximum contrast shows that the greatest variation of the reflection coefficient occurs in the red region of the spectrum during phase transition. This circumstance permits one to increase the visual contrast of the image by using radiation with specific spectral composition to illuminate the material. Thus, installation of the OS-13 light filter, which splits the blue-green region of the spectrum (Figure 2, 5) in front of the FTIROS lighting source increases the visual contrast of the images on the material up to a value of 0.73 without a significant loss of brightness coefficient.

Investigation of the angular characteristics of image brightness. We investigated the angular dependence of the brightness coefficients of FTIROS specimens on polished and ground sitall substrates by the method described in Section 1. The indicatrices of the brightness coefficient of thermochromic material FTIROS are presented in Figure 5 as a function of the observation angle. It is obvious from Figure 5 that the interference effects which determine the color of FTIROS have no effect on the angular distribution of the brightness coefficient and the brightness indicatrices are entirely determined by the quality of machining the surface of the material substrate. The use of FTIROS material on a ground substrate in display devices permits one to provide equal-brightness reading of information at

a wide angle of observation of approximately 110°. It should be noted that the value of the image brightness coefficient on FTIROS material depends only on the angle of observation and, unlike display devices based on non-mat liquid crystals [9], does not depend on the observation azimuth.

Conclusions

The investigations show that an image on thermochromic material FTIROS has good visual contrast and sufficient brightness coefficient for reflection of optical information on the material. These parameters in combination with reversibility and the possibility of accomplishing the non-volatile memory mode using the hysteresis effect during phase transition [1] indicate the promise of using the material in display equipment.

The authors are grateful to T. G. Lanskaya and V. O. Skvortsova for help in manufacturing the specimens and also to P. G. Golubev for useful discussion of the results of the paper.

BIBLIOGRAPHY

1. Zakharchenya, B. P., I. K. Meshkovskiy, Ye. I. Terukov and F. A. Chudnovskiy, PIS'MA ZHTF, Vol 1, No 8, 1975.

2. Chudnovskiy, F. A., ZHTF, Vol 45, 1975.

3. Oleynik, A. S., B. V. Abalduyev, B. P. Zakharchenya and F. A. Chudnovskiy, INZH.-FIZ. ZHURN., Vol 33, 1977.

4. Golubev, P. G., G. P. Skivko, T. G. Lanskaya, Ye. I. Terukov, F. A. Chudnovskiy and Z. I. Shteyngol'ts, PIS'MA ZHTF, Vol 1, 1975

5. Gurevich, M. M., "Tsvet i ego izmereniye" [Color and Measurement of It], Moscow, IZD-VO AN SSSR, 1950.

6. McAdam, D. L., J. OPT. SOC. AM., Vol 32, 1942.

7. Kelly, K. L., J. RES. NBS, Vol 31, 1943.

8. "Atlas standartnykh obraztsov tsveta, tip ATs-450" [Atlas of Standard Color Specimens, Type ATs-450], published by VNIIM imeni D. I. Mendeleyev, No 20076, 1970.

9. Barna, G. G., PRIBORY DLYA NAUCHNYKH ISSLEDOVANIY, No 10, 1976.

6521
CSO: 8344/519

PLASMA PHYSICS

UDC 537.533.7: 535.233.24

RELAXATION OF THE RELATIVISTIC ELECTRON BEAM IN A GAS, TAKING ACCOUNT OF THE RADIATION

Moscow DOKLADY AKADEMII NAUK SSSR in Russian Vol 248, No 1, 1979 pp 67-69

[Article by B.V. Alekseyev, A.S. Litvinovich and G.V. Neaterov, Moscow Aviation Institute imeni Sergo Ordzhonikidze; presented by Academician A.A. Drobnitsin]

[Text] Passage of a high-power relativistic electron beam (r.e.b.) through a gas is a high-temperature process ([1]) in which the transfer of radiant energy is determinant.

We consider the solution of the stationary axisymmetrical problem of r.e.b. relaxation in a dense gas. For the calculation of the r.e.b. relaxation a combined method has been developed based on the kinetic equation of radiation transport and the Monte Carlo method with the application of an iteration process.

The calculation of r.e.b. transmission against an assigned hydrodynamic background (as the first approximation) is performed by the method of statistical tests (a variant of the Monte Carlo method. The beam is simulated by an ensemble of particles. The computation algorithm is as follows: in conformity with the initial distribution function in phase space the electron coordinates and velocities at the moment of entry into the system are introduced, the length and time of the free path of the electron is calculated and its coordinates before the collision are found. The velocity of the atom participating in the collision is introduced. The electron velocity after the collision is determined from the conservation laws. The differential and total cross section for scattering of the electron by atoms and the effective excitation potential is calculated according to the formulas of Spencer and Bethe-Bloch respectively ([2]). Tracking of the electron is performed until it has lost most of its energy or left the region of interest.

The microparameters of the problem, and specifically the density of charged particles and the energy release function, in the computing cells of the region are obtained by averaging over the particle ensemble.

The calculation of the radiative transfer is carried out by the optimum method of spatial characteristic curves. The optimum situation is achieved by employing improved-accuracy quadratic Gauss formulas in calculation of the moments of the intensity I_ν of radiation into the solid angle ω at the frequency ν. The Planck distribution function B_ν is used as a weighting factor in the integration. The advisability of such a choice is indicated by the nature of the frequency dependence on the intensity of radiation. The radiation intensity I_ν at the computation points of the region in the directions $\underline{\omega}$, determined by the employed quadrature formulas, is found by solving the Cauchy problems for the transport equation

$$\underline{\omega} \nabla I_\nu = K (B_\nu - I_\nu).$$

The equation proposes that the condition of local thermodynamical equilibrium is fulfilled and scattering absent. The optical properties of the medium are given by the spectral coefficient of absorption K_ν which depends on the temperature T, pressure and frequency. A correct formulation of the problem calls for prescribed radiation intensities at the boundary of the region in inward directions.

The computation grid is formed by intersecting coordinate surfaces of the cylindrical coordinate system. The calculation of the radiation intensity, I_ν is performed along the characteristic curves $\underline{\omega}$ employing a tetrahedral pattern. A difference scheme is obtained by integrating the transport equation over the tetrahedron volumes. It is of the first order of approximation, monotonous and absolutely stable.

The problem considered here is a problem of radiation equilibrium in a closed cylindrical region. The energy released in the beam zone in a time unit is equal to the total radiant flux through the surface of the cylinder. The gas temperature in the volume is determined from the energy balance

$$\nabla q \quad Q,$$

where the divergence of the radiant flux q expresses the rate of the energy influx into a volume unit due to radiation, and Q the power released in a volume unit during the passage of the r.e.b.

The expression for ∇q is obtained by integrating the transport equation with respect to the solid angle and frequency. It is of the form

$$\nabla q = \frac{\sigma T^4}{\pi} 4\pi K_p - \frac{k T}{h} \int_0^\infty \int_{4\pi} K_\nu(x) I_\nu(x, \omega) d\omega dx;$$

here σ is the Stefan-Boltzmann constant, Kp the Planck-averaged coefficient of ansorption, and $x = h\nu/kT$.

Substituting the expression for ∇q into the condition of radiation equilibrium and solving the equation thus obtained with respect to T we obtain the iteration formula for calculation of the gas temperature at the grid points of the region

$$T_{(n+1)} = \left\{ \frac{1}{4\sigma K_p} \left[Q + \frac{kT}{h} \int_0^\infty \int_{4\pi} K_\nu(x) I_\nu(x, \omega) \, d\omega \, dx \right] \right\}^{1/4}_{(n)},$$

where n is the number of the iteration. These iterations will be called internal.

According to the approach adopted, the whole problem is subdivided into two independent stages - the relaxation process of the r.e.b. in the gas and the transfer of radiant energy. From the first stage with a fixed temperature field T the magnitude of the released energy Q is found; in the second stage with fixed energy release Q a new temperature field is computed. The problem is adjusted by an iteration procedure. The alternation of these stages will be called the external iterations.

Numerical calculations have been carried out for a cylindrical chamber of length 300 cm and radium 10 cm. The chamber is filled with potassium vapor at a pressure of 3 bar. The temperature of the chamber walls is kept constant at 2000K. It isassumed that the radiation from the walls into the chamber is perfect black-body radiation with the Planck distribution function. The r.e.b. of initial radius 1 cm, initial energy 0.2 MeV and power 0.4 MW enters into the chamber from the end face. The system is placed in an external longitudinal magnetic field of induction 50,000 Gauss. With these parameters the meam turns out to be magnetized so that the energy release is practically concentrated in the near-axis zone. To achieve convergence 15 external iterations were needed, the number of internal iterations in the second stage was 8. Improvement of convergence was attained by application of a damping procedure to the energy release function

$$Q^{m+1} = Q^m + \delta(Q^{m+1} - Q^m), \quad \delta = 0.5;$$

here m is the number of external iterations. The accuracy with which the number of external iterations was fixed depending on the temperature did not exceed 2.5%.

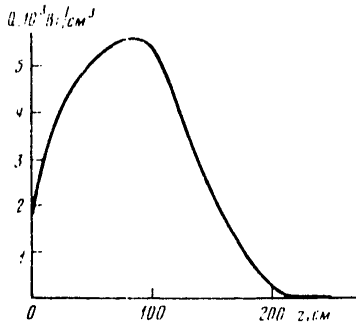

Fig. 1

z in cm

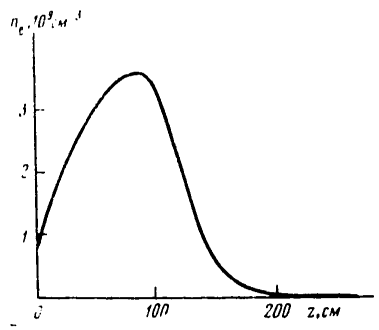

Fig. 2

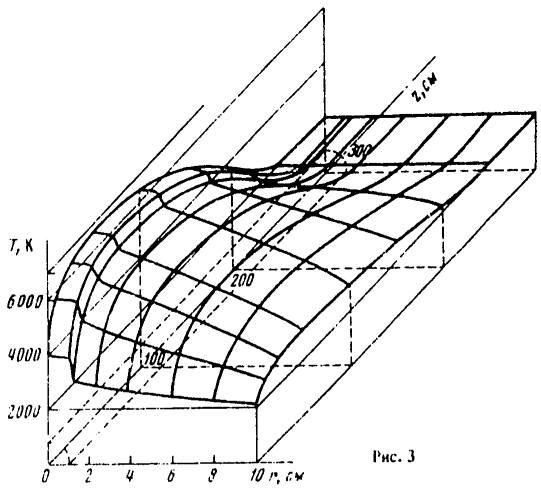

Рис. 3

Fig. 3

Fig. 1 shows the distribution of the rate of energy release, Fig. 2 that of the concentration of fast electrons (minimum energy 0.01 MeV) along the chamber axis. Fig. 3 represents the configuration of the temperature field in the chamber, the dashed line shows the beam zone. For a temperature of 6000°K the mean free path of the photons is 1 cm. Note the abrupt temperature gradient in the near-axis zone, which is connected with the formation of a beam channel.

Received 3-15-1979

BIBLIOGRAPHY

1. Iyevlev, V.M.; Koroteyev, A.S. et al., IZV. SO AN SSSR, No. 13, SER. TEKHN. NAUK, Vol 52, No 3, 1977.

2. Spencer, L. V., PHYS.REV., Vol 98, No 6, 1955.

3. Alekseyev, B.V., ZHURN. VICHISLIT. MATEM. I MATEM. FIZ., Vol 4, No 3, 1964

12157
CSO: 8144/0329

PLASMA PHYSICS

UDC 533.9

FEATURES OF THE HEATING OF A SUBSTANCE BY SPECIAL-FORM RADIATION

Moscow DOKLADY AKADEMII NAUK SSSR in Russian Vol 247, No 5, 1979
pp 1137-1140

[Article by V. K. Ablekov, Academician V. S. Avduyevskiy, Yu. N. Babayev, corresponding member of the USSR Academy of Sciences, and A. M. Frolov, submitted 4 Apr 79]

[Text] The problem of the heating of a substance by radiation is governed basically by the physics of the introduction of the electromagnetic energy and by the mechanisms of energy transfer from the electrons to the ions of the plasma of the substance.

In this article we look at the mechanism of the heating of ions of a dense plasma and a metal lattice relative to the energy of strong incident radiation.

The metal is treated as a "cold" plasma, i.e., kinetic effects of the electron gas are disregarded. The electron gas is considered degenerate up to temperature T_0 (T_0 is the degeneracy temperature). In connection with this the electrons close to the Fermi level are studied. The dispersion properties of plasma and metal are not taken into account. A spatially homogeneous formulation of the problem is investigated.

The electrons in the plasma and in the metal are in motion in a transverse wave field having the form

(1) $E = E_0 \sin \omega t.$

The motion of an electron in the field of a light wave satisfies the equation

(2) $$\frac{\partial u_e}{\partial t} = \frac{eE_0}{m_e} \sin \omega t - \nu_{ei} u_e,$$

where ν_{ei} is the frequency of the collision of electrons with ions or with the metal lattice. In the general case the collision frequency depends on the path velocity of the electrons.

Assuming that the reaction time is small in comparison with the time of propagation of the heat wave resulting from the heat-up of the electron gas, one can presume that heat-up of the electrons and the metal lattice is described by the equations

(3) $$c_e \frac{\partial T_e}{\partial t} = jE - \delta' \nu_{ei} (T_e - T_i),$$

(4) $$c_i \frac{\partial T_i}{\partial t} = \delta' \nu_{ei} (T_e - T_i), \quad \delta c_e = \delta',$$

where δ is the coefficient of elastic collision of the electrons and the lattice in the metal or of the electrons and the ions in the plasma. In the case of metals [1]

$$\delta = \frac{\pi^2}{6} \frac{m_e v_{Fe}^2 n}{c_e T} \gg 1,$$

and in the case of a plasma [2]

$$\delta = \frac{m_e}{m_i} \ll 1.$$

Assuming that δ is constant, i.e., is independent of the relative velocity of electrons and ions, we will obtain a solution of the system (1)-(4) in the form

(5) $$T_e - T_i = a \sin^2 \omega t + b \sin \omega t \cos \omega t + c \cos^2 \omega t;$$

(6) $$T_i = \delta \nu_{ei} \left(\frac{a+c}{2} t + \frac{B}{\omega} \sin^2 \omega t \right);$$

(7) $$a + c = \frac{e^2 n E_0^2}{m_e c_e \delta (\omega^2 + \nu_{ei}^2)},$$

where

(8) $$b = \delta^2 \frac{\nu_{ei}}{\omega} \frac{e^2 n E_0^2}{\delta m_e c_e (\omega^2 + \nu_{ei}^2)} \left(\frac{4\omega^2}{(4\omega^2 + \nu_{ei}^2 \delta^2)\delta} - \frac{\nu_{ei}^2 \delta}{(4\omega^2 + \nu_{ei}^2 \delta^2)} - \frac{1}{\delta} \right).$$

Averaging (5) and (6) with respect to time, we will derive from (5)-(8) the expressions

(9) $$T_e - T_i = \frac{e^2 n E_0^2}{\delta m_e c_e (\omega^2 + \nu_{ei}^2)},$$

$$(10)\quad T_1 = \delta^2 \frac{\nu_{ei}}{\omega} \frac{e^2 n E_0^2}{m_e c_e \delta (\omega^2 + \nu_{ei}^2)} \times$$
$$\times \left[\frac{\tau\omega}{2\delta} + \delta \frac{\nu_{ei}}{\omega} \left(\frac{4\omega^2}{(4\omega^2 + \nu_{ei}^2 \delta^2)\delta} + \frac{\nu_{ei}^2 \delta}{(4\omega^2 + \nu_{ei}^2 \delta^2)} - \frac{1}{\delta} \right) \right].$$

where τ is the effective time of the incident radiation. For the sake of simplicity, we will assume hereinafter that the effective time is equal in order of magnitude to the wave period. Solutions of (9) and (10) were obtained assuming the collision frequency to be independent of the temperature. However, these solutions can be the solutions in a zero approximation for the system (2)-(4) and for the case of collision frequency independence of temperature.

We will define now the conditions under which the dependence of collision frequency on temperature becomes significant.

From (2)-(4), when $\omega \ll \nu_{ei}$

$$(11)\quad T_e \frac{c_e}{n} \sim \frac{m_e \bar{V}^2}{2} \sim \frac{e^2 E_0^2}{\delta m_e \nu_{ei}^2} = \frac{1}{\delta} \frac{m_e u_e^2}{2}.$$

from which we find that, for plasma,

$$\bar{V}\sqrt{\delta} \sim u_e, \quad u_e \ll \bar{V},$$

since $\delta \ll 1$, and for metal $u_e \gg \bar{V}$, since $\delta \gg 1$.

When $\omega \gg \nu_{ei}$, we obtain a somewhat different expression

$$(12)\quad T_e \frac{c_e}{n} \sim \frac{m_e \bar{V}^2}{2} \sim \frac{e^2 E_0^2 \nu_{ei}}{m_e \delta \omega^2 (\omega + \delta\nu_{ei})}$$

and

$$(13)\quad \frac{m_e u_e^2}{2} \sim \frac{e^2 E_0^2 \nu_{ei}^2}{m_e \omega^4}.$$

Hence, we derive relationships having the form

$$(14)\quad \bar{V}\left(\frac{\delta\nu_{ei}(\omega + \delta\nu_{ei})}{\omega^2}\right)^{1/4} \sim u_e.$$

When $\omega \ll \delta\nu_{ei}$, we have from (14)

$$\bar{V}\sqrt{\frac{\delta\nu_{ei}}{\omega}} \sim u_e,$$

i.e., $u_e \gg V$ when $\delta \gg 1$. When $\omega \gg \delta\nu_{ei}$, where $\delta \gg 1$ or $\delta \ll 1$,

$$\bar{V}\sqrt{\frac{\delta\nu_{ei}}{\omega}} \sim u_e$$

and, consequently, $\bar{V} \gg u_e$.

Thus, the temperature dependence of the frequency of collision of electrons with ions is significant for metals only in the range of frequencies $\omega \gg \delta\nu_{ei}$, where $\delta \gg 1$, whereas for a plasma the dependence is significant for the entire range of frequencies [3].

Eliminating from (9) and (10) the electron temperature T_e and allowing for the relationship of ν_{ei} to T_e in a form $\nu_{ei} = \nu_0 (T_0/T_e)^{3/2}$ for $\delta \ll 1$ and $\nu_{ei} = \nu_0 (T_0/T_e)^{1/2}$, for $\delta \gg 1$, we will obtain for the case when $\omega \ll \nu_{ei}$ and $\delta \ll 1$

$$(15)\quad \left(\frac{T_i}{T_0}\right)^3 - 2\delta \frac{\omega^2}{\nu_0^2} \frac{T_i}{T_0}\left[\frac{T_i}{T_0} + \left(\frac{E_0^2}{E_p^2} - \frac{\nu_0^2}{\omega^2}\right)\right]\frac{E_0^4}{E_p^4} \quad 4\delta^4 \frac{\omega^2}{\nu_0^2}\frac{E_0^8}{E_p^8} = 0,$$

when $\nu_{ei} \ll \omega \ll \delta\nu_{ei}$, if $\delta \gg 1$,

$$(16)\quad \left(\frac{T_i}{T_0}\right)^3 \left(\frac{T_i}{T_0}\right)^2 \frac{E_0^2}{E_p^2} - \frac{\delta^2}{4}\frac{\nu_0^2}{\omega^2}\frac{E_0^4}{E_p^4} = 0$$

and when $\omega \gg \delta\nu_{ei}$, if $\delta \gg 1$,

$$\left(\frac{T_i}{T_0}\right)^3\left[\frac{E_0^2}{E_p^2} + \frac{T_i}{T_0}\right]^4 - 2\frac{T_i}{T_0}\left[\frac{E_0^2}{E_p^2} + \frac{T_i}{T_0}\right]^2 \frac{\nu_0^4\delta^4}{4\omega^4}\frac{E_0^2}{E_p} +$$
$$+ \frac{\nu_0^8\delta^8}{16\omega^6}\frac{E_0^4}{E_p^4} - \left[\frac{E_0^2}{E_p^2} + \frac{T_i}{T_0}\right]^3 \delta^2\frac{\nu^2}{\omega^4}\frac{E_0^4}{E_p^4} = 0,$$
$$E_p^2 = \delta m_e c_e \frac{T_0\omega^2}{c^2 n}.$$

where E_p^2 is the plasma parameter; δ is the coefficient of the collision of electrons with ions or with photons; T_0 is the initial temperature for the plasma or the degeneracy temperature of electron gas in the metal; ω is the frequency of the incident radiation; and ν_0 is the electron-ion collision frequency when $T_e = T_0$.

Figure 1 shows the general form of the relationship between the ion temperature T_i/T_0 and the intensity of the light field E_0/E_D for various ranges of radiation frequency: $\omega \ll \nu_{ei}$ (curve 1); $\nu_{ei} \ll \omega \ll \delta\nu_{ei}$ (2); $\omega \gg \delta\nu_{ei}$ (3).

A feature of these curves is their ambiguous quality in the region of energies less than E_p^2, connected with the instability of electron gas heat-up. The electron gas instability in this energy range was revealed earlier in reference [3]. It occurs in the region (0.1-10) E_p^2. The temperature of the ion subsystem in this case is of the order of magnitude of 10^5-10^7 K. For the region $\omega \ll \delta\nu_{ei}$ when $E_0^2 \gg E_p^2$, the temperature of the ion subsystem continues to increase (curve 1-rapidly, 2-slowly). In the region $\omega \gg \delta\nu_{ei}$ at higher incident radiation energies there is an ineffective dissipation of

energy, which is in accordance with a low efficiency of the collision mechanism of energy transfer from radiation to ion subsystem.

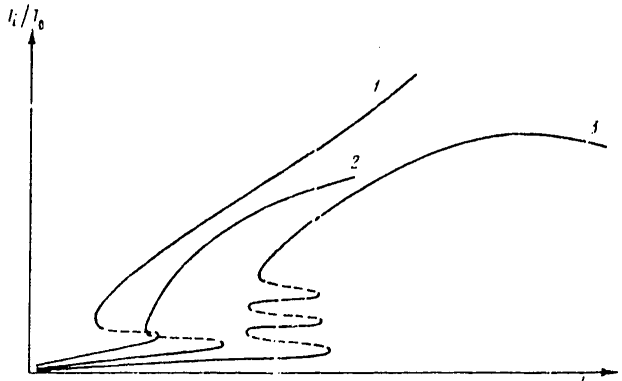

Figure 1

The nature of the instability governs the effective form of radiation for heating the substance. It should repeat the form of the curve in the region of instability since the instability can lead to cutoff of heating. This circumstance makes it possible, by means of further frequency modulation with the energy governed by the space between the two branches of instability, to ensure throwing the process into another stage. The profiled heating and the frequency modulation may contribute substantially to solving the problem of strong heating of matter treated in [4, 5].

BIBLIOGRAPHY

1. Kittel, C. "Quantum Theory of Solids," Nauka, 1967.

2. Spitzer, L. "The Physics of Fully Ionized Gases," Moscow, IL, 1957.

3. Ginzburg, V. L. "Rasprostraneniye elektromagnitnykh voln v plazme" [The Propagation of Electromagnetic Waves in Plasma], Moscow, Fizmatgiz, 1960.

4. Basov, N. G.; Gribkov, V. A. et al. ZHETF, Vol 54, 1968, p 1073.

5. Pashinin, P. P., and Prokhorov, A. M. ZHETF, Vol 62, 1972, p 189.

5454
CSO: 8144/0297

UDC 519.95

THE POLYNOMIAL SOLVABILITY OF CONVEX QUADRATIC PROGRAMMING

Moscow DOKLADY AKADEMII NAUK SSSR in Russian Vol 248 No 5, 1979 pp 1049-1051
manuscript received 20 Apr 79

[Article by M.K. Kozlov, S.P. Tarasov and L.G. Khachiyan, USSR Academy of Sciences Computer Center, Moscow; presented by Academician A.A. Dorodnitsyn, 16 Apr 79]

[Text] We shall consider the problem of convex quadratic programmin (k.p.) [QP]:

$$(1)\qquad f(x)=\frac{1}{2}(x, Cx)+(d, x)=\frac{1}{2}\sum_{i,j=1}^{n} c_{ij}x_ix_j+\sum_{j=1}^{n} d_jx_j \to \min,$$
$$(A_i, x)=\sum_{j=1}^{n} a_{ij}x_j \leqslant b_i;\quad i=1,2,\ldots,m;\ x\in R^n,$$

where C is an integer symmetrical positive semi-definite matrix, and the vectors d and A_i, and the scalars b_i are also integral.

The following quantity is termed the input length of the QP problem:

$$(2)\qquad L=L_1+L_2=\left[\sum_{i,j=1}^{n}\log_2(|c_{ij}|+1)+\sum_{j=1}^{n}\log_2(|d_j|+1)\right]+$$
$$+\left[\sum_{i,j=1}^{m,n}\log_2(|a_{ij}|+1)+\sum_{i=1}^{m}\log_2(|b_i|+1)+\log_2 nm+1\right],$$

which defines the number of binary symbols necessary for writing (encoding) the input information of the problem.

The following is understood to be the precise solution of the QP problem:

a) The determination of the compatibility of the system of linear inequalities; in the case of compatibility, the determination of whether the functional f(x) is limited on the downside in the set $X \subseteq R^n$ of solutions of the system of inequalities;

b) If the limitations are compatible and the functional is limited in X, then the finding of the extremal value $f^o = t/s$ (t and s are mutually prime

integers, as well as the rational vector $x^0 \in X$, where the extremum is achieved.

An algorithm is constructed in this paper for the precise solution of the QP problem, the labor intensity of which is limited by a polynomial of input length L, i.e., it is demonstrated that the QP belongs to a class of problems P which are solvable in determinate Turing machines in a time polynomial with respect to the input [1]. We shall now move on to the construction of the algorithm.

I. An algorithm T was constructed in [2] to determine the compatibility in R^n systems of the linear inequalities:

$$(A_i, x) \leqslant b_i, \quad i = 1, 2, \ldots, m,$$

with a labor intensity L_2, polynomial with respect to the input, where L_2 i defined by formula (2). The characteristics of the algorithm T are as follows: a memory of $O(n^2 + nm)$ numbers, each of which has a fixed decimal point $O(nL_2)$ for the bits written in the binary system; $O(n^3(n^2 + m)L_2)$ elementary addition, subtraction, multiplication, division, square root, max. and min. operations are performed on numbers with a precision of $O(nL_2)$ digits.

Thus, the compatibility of the system of linear inequalities - the limitations of the QP problem is tested by algorithm T. It is assumed below that $X \neq \phi$.

The downside limitation of the convex quadratic functional on X is equivalent to the compatibility of a system of n + m linear inequalities and equalities in terms of the variables $(x, \lambda) \in R^{n+m}$

$$\begin{aligned} &Cx + d + \sum_{i=1}^{m} \lambda_i A_i = 0, \\ &\lambda_i \geqslant 0, \quad i = 1, 2, \ldots, m. \end{aligned} \tag{3}$$

The input of system (3) does not exceed 2L, where L is the input of the QP problem. For this reason, the compatibility of system (3) and consequently also the downward limitation of f(x) in X is checked by algorithm T with a labor intensity polynomial with respect to L. For this, $O((n + m)^5 L)$ elementary operations are required on $O((n + m)L)$ digit numbers. Thus, according to section (a), the precise solution of the QP problem is exhausted. In the following the downward limitation of f(x) in X is assumed. With these assumptions, the minimum of the quadratic functional is achieved, in which case, it can be shown that the optimum value has the form $f^0 = t/s$, where t and s are mutually prime integers, $|t| \leq 2^{5L}$, $|s| \leq 2^{4L}$.

II. We shall show that to precisely find the optimal value $f^0 = t/s$ of the functional, it is sufficient to determine the compatibility of 13L + 2 systems, P_k, of the form:

$$\begin{aligned} &(A_i, x) \leqslant b_i, \quad i = 1, 2, \ldots, m, \\ &f(x) \leqslant t_k/s_k, \end{aligned}$$

in which case, the integers t_k and s_k, which specify the system P_k, $k = 1, 2, \ldots, 13L + 2$, do not exceed the absolute value $|t_k| \leq 2^{13L+2}$, $|s_k| \leq 2^{8L+2}$. In fact, since $f^0 \in [-2^{5L}, 2^{5L}]$, then by using the method of dividing the segment $[-2^{5L}, 2^{5L}]$ in half, and checking in each step the compatibility of the system P_k with the corresponding t_k and s_k, once can find the approximate value of f^0 within a precision of 2^{-8L-2} over $13L + 2$ steps, i.e., a number $f = t_{13L+2}/s_{13L+2}$ can be found such that:

$$|f - f^0| = |f - t/s| \leq 2^{-8L-2}, \quad |s| \leq 2^{4L}. \tag{4}$$

It follows from (4) that the fraction t/s is the convergent of the continued fraction of the number f, and can be found by the expansion of f in a continued fraction. Thus, the precise value of f^0 is found from the approximated f over a time polynomial in L: for this, O(L) addition, subtraction, multiplication, division, and max operations required, which are performed with a precision of O(L) digits on O(L) digit numbers.

III. We shall now construct the algorithm, polynomial with respect to L, for the determination of the compatibility in R^n of an arbitrary system P_k, $k = 1, 2, \ldots, 13L + 2$, specified by integers t_k and s_k, $|t_k| \leq 2^{13L+2}$, $|s_k| \leq 2^{8L+2}$. For this, two lemmas are required, which are similar to lemmas 1 and 2 from [2].

Lemma 1. If the system P_k is compatible (i.e. $t_k/s_k \geq t/s$, then there exists its solution from the Euclidean sphere $S = \{x \mid \|x\| \leq 2^{2L}\}$.

Let $$\theta(x) = \max |f(x) - t_k/s_k, (A_i, x) - b_i|, \quad i = 1, 2, \ldots, m,$$

be the disparity of the system P_k at the point $x \in R^n$. In particular, $\theta(x) \leq 0$, then and only then is x a solution of P_k.

Lemma 2. If the system P_k is disjoint (i.e., $t_k/s_k < t/s$), then for any $x \in R^n$, the disparity is $\theta(x) > 2 \cdot 2^{-15L}$.

As soon as Lemmas 1 and 2 have been established, the same arguments as were employed in [2] to determined the compatibility of the systems of linear inequalities can be used to construct the polynomial algorithm for the determination of the compatibility of the systems P_k. It follows from the lemmas that to determine the compatibility in R^n of an arbitrary system P_k, it is sufficient to find such a point $x \in R^n$ that:

$$\theta(x) \leq \theta_S + 2^{-15L}, \tag{5}$$

where θ_S is the minimum of the disparity of the system P_k on the sphere S. In actual fact, in this case we have either $\theta(x) \leq 2^{-15L}$ (the system P_k is compatible), or $\theta(x) \geq 2 \cdot 2^{-15L}$ (the system is disjoint). In turn, one can make use of the algorithm of ellipsoids [2, 3] to find the requisite point x which satisfies (5). The characteristics of this algorithm are as

follows in our case: to determine the compatibility of each of the systems P_k, a memory of $O(n^2 + nm)$ numbers is required with a written length of $O(nL)$ bits; $O(n^3(n^2 + m)L)$ elementary operations with a precision of $O(nL)$ digits are performed on these numbers.

Thus, in sections II and III, an algorithm polynomial with respect to L is constructed for the determination of the extremal value of a convex quadratic functional for the case of linear limitations.

IV. Let the optimum value of the functional $f^0 = t/s$, $|t| \leqslant 2^{\varphi L}$, $|s| \leqslant 2^{\varphi L}$, be found. To find a certain optimal point of the QP problem, it is sufficient to find the vector $x^0 \in R^n$ which satisfies the system:

$$(U_1) \qquad \begin{aligned} &(A_i, x) \leqslant b_i, \quad i = 1, 2, \ldots, m, \\ &f(x) \leqslant t/s. \end{aligned}$$

The solution of this compatible system can be obtained in the folling manner. Let $X_1 \subseteq R^n$ be a set of solutions of the system U_1. In it, we replace the linear inequality $(A_1,x) \leq b_1$ which comes first in terms of the order of magnitude by the equality $(A_1,x) = b_1$, and determine the compatibility of the system obtained as a result of this substitution. If it is disjoint, then the first linear limitation in U_1 is redundant (since the hyperplane defined by this linear limitation does not intersect X_1) and is rejected. Otherwise, the equality in the first line is registered. The system U_2 resulting in this manner has a nonempty set of solutions X_2 X_1, and in this case, the total number of limitations in U_2 has not increased, while the number of linear limitations - inequalities has been reduced by unity. We then replace the inequality $(A_2,x) \leq b_2$, which is first in terms of the order of magnitude, by the equality, determine the compatibility of the system resulting following the substitution, etc. After m steps, we obtain the compatible system U_{m+1}, consisting of only linear equalities and the quadratic inequality, $f(x) \leq t/s$. Taking into account the fact that the point where the minimum of the quadratic functional is reached at $r, 0 \leq r \leq m$, linear limitations -- equalities with integral coefficients, is found over a time polynomial in L, we obtain the precise solution of the QP problem.

BIBLIOGRAPHY

1. S.A. Kuk, "Kibernetichnyy sbornik, novaya seriya" ["Collected Cybernetics Papers, New Series"], Vol 12, Moscow, Mir Publishers, 1975, p 5.

2. L.G. Khachiyan, DAN [REPORTS OF THE USSR ACADEMY OF SCIENCES], Vol 244, No 5, p 1093 (1979).

3. D.B. Yudin, A.S. Nemirovskiy, EKONOMIKA I MATEMATICHESKIYE METODY [ECONOMICS AND MATHEMATICAL METHODS], Vol 12, No 2, p 357 (1976).

[51-8225]

8225
CSO: 1862

CYBERNETICS

UDC 519.95

A POLYNOMIAL ALGORITHM IN LINEAR PROGRAMMING

Moscow DOKLADY AKADEMII NAUK SSSR in Russian Vol 244 No 5, 1979 pp 1093-1096 manuscript received 4 Oct 78

[Article by L.G. Khachiyan, Computer Center of the USSR Academy of Sciences, Moscow, presented by academician A.A. Dorodnitsyn, 4 Oct 78]

[Text] We shall consider a system of $m \geq 2$ linear inequalities with respect to $n \geq 2$ real variables $x_1, \ldots, x_j, \ldots, x_n$:

$$a_{i1}x_1 + \ldots + a_{in}x_n \leq b_i, \quad i = 1, 2, \ldots, m, \tag{1}$$

with integer coefficients a_{ij} and b_i. Let

$$L = \left[\sum_{i,j=1}^{m,n} \log_2 (|a_{ij}|+1) + \sum_{i=1}^{m} \log_2 (|b_i|+1) + \log_2 nm \right] + 1 \tag{2}$$

is the length of the system input, i.e., the number of 0 and 1 symbols needed to write (1) in binary notation.

In this paper, an alogrithm polynomial with respect to L is constructed for the determination of the compatibility or incompatibility in R^n of the arbitrary system (1). This algorithm requires a memory of $O(nm + n^2)$ numbers, each of which has O(nL) digits in binary notation. $O(n^3(n^2 + m)L)$ addition, subtraction, multiplication, division, square root and max. operations are performed on these numbers, where the requisite precision in executing the operations is O(nL) digits. In other words, it is proved that the problem proved that the problem of determining the compatibility of the systems of linear inequalities in R^n belongs to a class P of problems which are polynomially solvable [1] in determinate Turing machines. The polynomial solvability of linear programming problems likewise follows from this result, i.e., problems of linear form maximization with integer coefficients for the case of the limitations of (1). It should likewise be noted that the question of the completeness of the problem of determining the compatibility of systems of linear inequality in the class of NP problems was also posed in [1]. Thus, this problem is either incomplete or P = NP.

1. The Localization of the Solutions and the Incompatibility Measure.

Lemma 1. If the system (1) with the input L is compatible, then there exists a solution x^0 from the Euclidian of the sphere $S = \{x \mid \|x\| \leqslant 2^L\}$.

Let

$$\theta(x) = \max\{a_{i1}x_1 + \ldots + a_{in}x_n - b_i\}, \quad i = 1, 2, \ldots, m, \tag{1.1}$$

$\theta(x)$ is the disparity of the system at the point $x \in R^n$. We will note that if x^0 is a solution of the system, then $\theta(x^0) \leq 0$.

Lemma 2. If the system (1) with the input L is incompatible, then for any $x \in R^n$, the disparity $\theta(x) \geq 2 \cdot 2^{-L}$.

It follows from lemmas 1 and 2 that to solve the problem of the compatibility of system (1), it is sufficient to find a point x in R^n such that $\theta(x) \leq \theta_S + 2^{-L}$, where θ_S is the minimum of the disparity on the sphere S. In actual fact, in this case, we have either $\theta(x) \leq 2^{-L}$ (the system is compatible) or $\theta(x) \geq 2 \cdot 2^{-L}$ (the system is incompatible).

A description of an algorithm for finding the requisite point x where the algorithm is polynomial with respect to L is given in section 3. This algorithm is based on concepts close to the method of ellipsoids of N.Z. Shor [2, 3]. However, a few auxiliary constructions are required first.

2. Auxiliary Constructions. We shall consider an ellipsoid E in R^n, specified by the pair (x, Q), where $x \in R^n$ is the center of the ellipsoid and $Q = \|q_{ij}\|$ is an (n x n) matrix. This ellipsoid represents the mapping of the Euclidian of the pair $\|z\| \leq 1$ shifted to the point x with the transformation Q, i.e., $E = \{y \mid y = x + Qz, \ \|z\| \leq 1\}$. In particular, E is not degenerate if *det* $Q \neq 0$. We shall set $\|Q\| = \sqrt{\Sigma q_{ij}^2}$ and we shall say that the ellipsoid $E' \simeq (x', Q')$ approximates the ellipsoid $E \simeq (x, Q)$ with a precision of δ if $\|x' - x\| + \|Q' - Q\| \leq \delta$.

Let the nondegenerate ellipsoid $E \simeq (x, Q)$ and the nonzero n-dimensional vector R be given. We shall designate the figure (semi-ellipsoid) obtained by the intersection of E with the half-space $R^T(y - x) \geq 0$ as $(1/2)E_R$.

Lemma 3. Let $E \simeq (x, Q)$ be a nondegenerate ellipsoid and $(1/2)E_R$ $(R \neq 0)$ be its semi-ellipsoid. We shall consider the ellipsoid $E^R \simeq (x^R, Q^R)$:

$$x^R = x + \frac{QQ^TR}{(n+1)\|Q^TR\|}, \quad Q^R = 2^{1/8n^2} \cdot Q \cdot \mathrm{ORT}(Q^TR) \cdot \Lambda_n, \tag{2.1}$$

where $ORT(Q^TR)$ is an orthogonal (n x n) matrix, the first column of which is the vector $Q^TR/\|Q^TR\|$, while Λ_n is a diagonal (n x n) matrix,

$$\Lambda_n = \operatorname{diag}\left(\frac{n}{n+1}, \frac{1}{\sqrt{1-1/n^2}}, \ldots, \frac{1}{\sqrt{1-1/n^2}}\right). \tag{2.2}$$

If the ellipsoid $E' \supseteq (x', Q')$ serves as a δ-approximation for E^R, in which case:

$$\delta \leqslant n^{-1/n} \frac{|\det Q|}{\|Q\|^{n-1}}, \tag{2.3}$$

Then E' completely contains in itself the semi-ellipsoid $(1/2)E_R$ and

$$\|x'\| \leqslant \|x\| + \frac{\|Q\|}{n}, \quad \|Q'\| \leqslant \|Q\| \cdot 2^{1/n^2}, \tag{2.4}$$

$$2^{-1/n} \leqslant \det Q'/\det Q \leqslant 2^{-1/4n}. \tag{2.5}$$

The sense of Lemma 3 consists in the fact that it permits an analytical circumscription of the new ellipsoid E' about the semi-ellipsoid $(1/2)E_R$ so that: a) Only appropriate calculations are used; b) The valuations of the quantities $\|x'\|$ and $\|Q'\|$ do not exceed the valuations $\|x\|$ and $\|Q\|$ by too much; c) The ratio of the volumes of the ellipsoids $\text{mes}E'/\text{mes}E = \det Q'/\det Q$ falls within the limits of (2.5).

3. The Description of the Algorithm. We shall write the original system of linear inequalities (1) in the form:

$$A_i^T x \leqslant b_i, \quad i = 1, 2, \ldots, m, \tag{3.1}$$

where A_i are the rows of the system. Without limiting the generality, we shall assume that all $A_i \neq 0$. The operation of the algorithm consists of $N = 16n^2L$ iterations with numbers $k = 0, 1, \ldots, N$. At the k-th iteration, we have: an ellipsoid $E_k \supseteq (x_k, Q_k)$ and a scalar θ_k. In "physical" terms, x_k, Q_k and θ_k take the form of data files, each scalar component of which is written in binary notation on a tape M, having 23L bits ahead of the decimal point and 38nL bits after it. We shall say that the scalar θ fits on the tape M if $\|\theta\| \leq 2^{23L}$. Similarly, the data files x and Q fit on tapes M if each scalar element of them fits in. For this, it is sufficient that $\|x\|$, $\|Q\| \leq 2^{23L}$.

In the initial iteration with the number k = 0, we write:

$$x_0 = 0, \quad Q_0 = \operatorname{diag}(2^L, \ldots, 2^L), \quad \theta_0 = \max\{-b_i\}, \tag{3.2}$$

i.e. the ellipsoid E_0 coincides with the sphere S, while θ_0 is the amount of the disparity at the center of the sphere. The following inequalities are justified in the k-th iteration:

$$\|x_k\| \leq \frac{k}{n} 2^{18L}, \quad \|Q_k\| \leq 2^{2L+k/n^2}, \quad |\theta_k| \leq 2^{23L}; \tag{3.3}$$

$$2^{nL-k/n} \leq \det Q_k \leq 2^{nL-k/4n}. \tag{3.4}$$

In particular, since $k \leq 16n^2L$, it follows from (3.3) and (3.4) that x_k, Q_k and θ_k all fit on the tapes M. When $k = 0$, the inequalities (3.3) and (3.4) are obvious, and the proof for other values of $k \leq N$ is accomplished using induction.

The operation of the algorithm in the k-th iteration begins with the fact that the disparity $\theta(x_k)$ is computed in the center of the next ellipsoid E_k. Since $\|A_i\|, |b_i| \leq 2^L$ and the vectors A_i are integral, ti follows from (3.3) that the quantity $\theta(x_k)$ can be found precisely and will fit in M. In an analogous manner, the number i_k of the row in which the maximum of (1.1) is achieved at the point $x = x_k$ is found precisely. It is then assumed that $\theta_{k+1} = \min(\theta_k, \theta(x_k))$. The quantity θ_{k+1} which can be computed precisely represents the record minimum value of the disparity in the already obtained approximations $x_0, \ldots, x_k$ and satisfies (3.3) for the case of k+1, since this inequality is true for k.

We then go about finding the new ellipsoid $E_{k+1} = (x_{k+1}, Q_{k+1})$, which entirely encompasses the semi-ellipsoid $(1/2)E_k$, which is obtained from the E_k intercept of the region $A(x-x_k) > 0$, in which the disparity $\theta(x)$ knowingly exceeds $\theta(x_k)$. For this, the vector $F_k = -Q_k A_{ik}^T$ is found again, which by virtue of the integer nature of A_{ik} and (3.3) can be computed precisely and fits on the tapes M. Obviously, $F_k \neq 0$, since $A_{ik} \neq 0$, and it follows from (3.4) that $\det Q_k \neq 0$. In having the precisely found $F_k \neq 0$, E_{k+1} is computed from formulas similar to (2.1):

$$x_{k+1} \approx x_k + \frac{Q_k F_k}{(n+1)\|F_k\|}, \quad Q_{k+1} \approx 2^{1/8n^2} \cdot Q_k \operatorname{ORT}(F_k) \Lambda_n, \tag{3.5}$$

and in this case, these calculations are carried out in an approximate fashion with a precision of $\delta = 2^{-37nL}$. (We recall that the tape M has 38nL digits after the decimal point). However, it is important to note the following: since $\|Q_k\| \leq 2^{23L}$, $O(n^3)$ addition, subtraction, multiplication, division, square root and max.operations are sufficient for the calculations of (3.5) with a precision of $\delta = 2^{-37nL}$, where these operations can be carried out with a precision of O(nL) digits.

With this, the k-th iteration is completed. If $k < 16n^2L$, we set about the (k+1)th iterations; however, if $k = 16n^2L$, the count is terminated and the record minimum disparity θ_{N+1} is fed to the output.

The description of the algorithm is actually completed, and it is only necessary to inductively prove inequalities (3.3) and (3.4) for the case of k+1, assuming they are justified for the case of k. This proof is easily derived from Lemma 3.

Theorem 1. The record minimum value of the disparity θ_{N+1} satisfies the inequality $\theta_{N+1} \leq \theta_S + 2^{-L}$, where θ_S is the minimum of the disparity on the sphere S.

It follows from Theorem 1 and the results of section 1 that either $\theta_{N+1} \leq 2^{-L}$ (system (1) is compatible), or $\theta_{N+1} \geq 2 \cdot 2^{-L}$ (the system is incompatible). The requisite polynomial algorithm has been constructed.

BIBLIOGRAPHY

1. R.M. Karp, "Kibernetich. sb., Nov. Ser." ["Collected Papers in Cybernetics, New Series"], No 12, 16 (1975).

2. D.B. Yudin, A.S. Nemirovskiy, EKONOMIKA I MATEMATICH. METODY [ECONOMICS AND MATHEMATICAL METHODS], Vol 12, No 2, p 357 (1976).

3. N.Z Shor, KIBERNETIKA, No 2, p 80 (1970).

[47-8225]

8225
CSO: 1862

- END -